ORIGINAL RESEARCH ARTICLE

Endothelial HDAC1-ZEB2-NuRD Complex Drives Aortic Aneurysm and Dissection Through Regulation of Protein S-Sulfhydration

Shanshan Luo, PhD*; Chuiyu Kong, PhD*; Shuang Zhao, PhD*; Xin Tang, PhD*; Yu Wang, MSc; Xuechun Zhou, MSc; Rui Li, MSc; Xingeng Liu, MSc; Xinlong Tang, MD, PhD; Shixiu Sun, MSc; Wei Xie, MSc; Zhi-Ren Zhang ⓘ, MD, PhD; Qing Jing ⓘ, PhD; Aihua Gu, PhD; Feng Chen ⓘ, MD, PhD; Dongjin Wang, MD, PhD; Hong Wang ⓘ, MD, PhD†; Yi Han ⓘ, MD, PhD†; Liping Xie ⓘ, MD, PhD†; Yong Ji ⓘ, MD, PhD†

BACKGROUND: Aortic aneurysm and aortic dissection (AAD) are life-threatening vascular diseases, with endothelium being the primary target for AAD treatment. Protein S-sulfhydration is a newly discovered posttranslational modification whose role in AAD has not yet been defined. This study aims to investigate whether protein S-sulfhydration in the endothelium regulates AAD and its underlying mechanism.

METHODS: Protein S-sulfhydration in endothelial cells (ECs) during AAD was detected and hub genes regulating homeostasis of the endothelium were identified. Clinical data of patients with AAD and healthy controls were collected, and the level of the cystathionine γ lyase (CSE)/hydrogen sulfide (H_2S) system in plasma and aortic tissue were determined. Mice with EC-specific CSE deletion or overexpression were generated, and the progression of AAD was determined. Unbiased proteomics and coimmunoprecipitation combined with mass spectrometry analysis were conducted to determine the upstream regulators of the CSE/H_2S system and the findings were confirmed in transgenic mice.

RESULTS: Higher plasma H_2S levels were associated with a lower risk of AAD, after adjustment for common risk factors. CSE was reduced in the endothelium of AAD mouse and aorta of patients with AAD. Protein S-sulfhydration was reduced in the endothelium during AAD and protein disulfide isomerase (PDI) was the main target. S-sulfhydration of PDI at Cys343 and Cys400 enhanced PDI activity and mitigated endoplasmic reticulum stress. EC-specific CSE deletion was exacerbated, and EC-specific overexpression of CSE alleviated the progression of AAD through regulating the S-sulfhydration of PDI. ZEB2 (zinc finger E-box binding homeobox 2) recruited the HDAC1-NuRD complex (histone deacetylase 1–nucleosome remodeling and deacetylase) to repress the transcription of *CTH*, the gene encoding CSE, and inhibited PDI S-sulfhydration. EC-specific HDAC1 deletion increased PDI S-sulfhydration and alleviated AAD. Increasing PDI S-sulfhydration with the H_2S donor GYY4137 or pharmacologically inhibiting HDAC1 activity with entinostat alleviated the progression of AAD.

CONCLUSIONS: Decreased plasma H_2S levels are associated with an increased risk of aortic dissection. The endothelial ZEB2-HDAC1-NuRD complex transcriptionally represses *CTH*, impairs PDI S-sulfhydration, and drives AAD. The regulation of this pathway effectively prevents AAD progression.

Key Words: aortic aneurysm ■ aortic dissection ■ endothelium

Correspondence to: Yong Ji, MD, PhD, Key Laboratory of Cardiovascular and Cerebrovascular Medicine, Key Laboratory of Targeted Intervention of Cardiovascular Disease, Collaborative Innovation Center for Cardiovascular Disease Translational Medicine, the Affiliated Suzhou Hospital of Nanjing Medical University, Gusu School, Nanjing Medical University, 101 Longmian Ave, Jiangning District, Nanjing, 211166, Jiangsu, China, Email yongji@njmu.edu.cn or Liping Xie, MD, PhD, Key Laboratory of Targeted Intervention of Cardiovascular Disease, Collaborative Innovation Center for Cardiovascular Disease Translational Medicine, Nanjing Medical University, 101 Longmian Ave, Jiangning District, Nanjing, 211166, Jiangsu, China, Email lipingxie@njmu.edu.cn or Yi Han, MD, PhD, Department of Geriatrics, First Affiliated Hospital of Nanjing Medical University, 300 Guangzhou Rd, Nanjing, Jiangsu, China, Email hanyi@jsph.org.cn or Hong Wang, MD, PhD, Center for Metabolic Disease Research, Department of Microbiology and Immunology, Temple University, Lewis Katz School of Medicine, Medical Education & Research Building, 3500 N Broad St, Philadelphia, PA 19140, Email hongw@temple.edu

*S. Luo, C. Kong, S. Zhao, and X. Tang contributed equally.

†H. Wang, Y. Han, L. Xie, and Y. Ji contributed equally.

Supplemental Material is available at https://www.ahajournals.org/doi/suppl/10.1161/CIRCULATIONAHA.122.062743.

For Sources of Funding and Disclosures, see page XXX.

Clinical Perspective

What Is New?

- We discovered that S-sulfhydration of protein disulfide isomerase is crucial for preventing aortic aneurysm and dissection (AAD) through maintenance of endothelial cell homeostasis.
- The ZEB2-HDAC1-NuRD complex (zinc finger E-box binding homeobox 2–histone deacetylase 1–nucleosome remodeling and deacetylase) reduces the S-sulfhydration of protein disulfide isomerase by repressing the cystathionine γ lyase (CSE)/hydrogen sulfide (H_2S) system and contributes to the initiation of AAD.
- Lower plasma H_2S levels are associated with an increased risk of aortic dissection.

What Are the Clinical Implications?

- The ZEB2-HDAC1-NuRD complex and CSE/H_2S axis may serve as novel therapeutic targets for managing AAD.
- Pharmacological or genetic regulation of the ZEB2-HDAC1-NuRD complex or CSE/H_2S system can alleviate AAD progression.
- Reduced plasma H_2S concentration may serve as an independent risk factor for AAD.

Nonstandard Abbreviations and Acronyms

3-MA	3-methyladenine
AAA	abdominal aortic aneurysm
AAD	aortic aneurysm and aortic dissection
AAV	adeno-associated virus
Ang II	angiotensin II
ANS	1-anilinonaphthalene-8-sulfonic acid
AoD	aortic dissection
ATF6	activated transcription factor 6
BMI	body mass index
CBS	cystathionine β-synthase
CSE	cystathionine γ lyase
CTBP	C-terminal binding protein
CXXC	Cys-Xaa-Xaa-Cys
EC	endothelial cell
eIF2a	eukaryotic initiation factor 2a
ER	endoplasmic reticulum
GFP	green fluorescent protein
H2S	hydrogen sulfide
HA	human influenza hemagglutinin
HDAC1	histone deacetylase 1
HUVEC	human umbilical vein endothelial cell
IRE1	inositol-requiring 1
KEAP1	Kelch-like ECH-associated protein 1

NRF2	nuclear factor erythroid 2–related factor 2
NuRD	nucleosome remodeling and deacetylase
OR	odds ratio
PDI	protein disulfide isomerase
PDI-SSH	S-sulfhydration of protein disulfide isomerase
PERK	protein kinase RNA-like endoplasmic reticulum kinase
PTM	posttranslational modification
SBP	systolic blood pressure
SUMO1	small ubiquitin-like modifier 1
TRIM21	tripartite motif containing 21
WT	wild-type
ZEB2	zinc finger E-box binding homeobox 2

The aortic cells and extracellular matrix are highly dynamic in response to changes in the humoral and biomechanical environment. The integrity of the vascular endothelium is necessary for the structural and functional homeostasis of the vasculature.[1] Aberrant regulation of aortic components leads to aortic degeneration, biomechanical failure, and development of aortic aneurysm and aortic dissection (AAD).[2] Endovascular aortic or open surgical repair is used widely for the treatment of AAD. However, a large number of patients experience persistent aortic degeneration that requires further pharmacological intervention.[3] Medications for the prevention and treatment of AAD are limited and the effects of beta-blockers and angiotensin II (Ang II) type 1 receptor blockers on AAD treatment are controversial.[4–7] Therefore, a better understanding of the pathogenesis of AAD at the molecular level is necessary to explore potential medications for AAD and improve the prognosis of patients with AAD who undergo surgical treatment.

The mechanisms underlying AAD development are complex. Apart from genetic mutations that influence the vascular structure and cellular connection, inflammation, dysfunction of the vascular smooth muscle cells, and destruction of the extracellular matrix are considered causes of sporadic AAD. Endothelial function has a profound effect on vascular physiology and pathology. Multiple lines of evidence recently suggested that endothelial dysfunction plays an important role in the development of aortic aneurysms. Ang II type 1a deficiency in the endothelial cells (ECs), rather than in the smooth muscle or bone marrow−derived cells, attenuates the development of ascending aortic aneurysms.[8] Moreover, endothelial dysfunction is an early event in abdominal aortic aneurysm (AAA) in Nox2 transgenic mice.[9] Reestablishment of the endothelial lining can relieve aortic wall destruction and eventually stabilize aortic aneurysms, further

Table 1. Clinical Characteristics of Patients With Aortic Dissection and Healthy Controls

Characteristics	Controls (n=100)	All patients (n=99)	Aortic dissection			P value
			DeBakey I (n=68)	DeBakey II (n=7)	DeBakey III (n=24)	
Age, y	49.9±10.1	54.0±13.7	55.6±13.6	59.4±11.5	47.9±13.2	0.016
Male	81 (81.0)	80 (80.8)	52 (76.5)	7 (100.0)	21 (87.5)	0.973
BMI, kg/m²	26.6±3.28	25.0±3.85				0.068
<25	37 (37.0)	52 (52.5)	36 (52.9)	6 (85.7)	10 (41.7)	–
25 to <30	53 (53.0)	37 (37.4)	26 (38.2)	1 (14.3)	9 (37.5)	–
≥30	10 (10.0)	10 (10.1)	6 (8.8)	0 (0.0)	5 (20.8)	–
Risk factors						
Smoking	36 (36.0)	26 (26.3)	17 (25.0)	2 (28.6)	7 (29.2)	0.138
Hypertension	26 (26.0)	73 (73.7)	48 (70.6)	7 (100.0)	18 (75.0)	<0.001
Diabetes	12 (12.0)	7 (7.1)	5 (7.4)	1 (14.3)	1 (4.2)	0.237
Extent of aortic dissection						
Ascending aorta	–	75 (75.8)	68 (100.0)	7 (100.0)	0 (0.0)	–
Aortic arch	–	68 (68.7)	68 (100.0)	0 (0.0)	0 (0.0)	–
Descending aorta	–	82 (82.8)	68 (100.0)	0 (0.0)	14 (58.3)	–
Abdominal aorta	–	47 (47.5)	29 (42.7)	0 (0.0)	18 (75.0)	–
Iliac arteries	–	27 (27.3)	21 (30.9)	0 (0.0)	6 (25.0)	–
Patient history						
Marfan syndrome	–	1 (1.0)	1 (1.5)	0 (0.0)	0 (0.0)	–
Myocardial ischemia	–	8 (8.1)	6 (8.8)	1 (14.3)	1 (4.2)	–
CAD	–	2 (2.0)	2 (2.9)	0 (0.0)	0 (0.0)	–
AVR/MVR	–	2 (2.0)	2 (2.9)	0 (0.0)	0 (0.0)	–
Atrial fibrillation	–	3 (3.0)	3 (4.4)	0 (0.0)	0 (0.0)	–
Stroke	–	2 (2.0)	1 (1.5)	0 (0.0)	1 (4.2)	–
Renal dialysis	–	3 (3.0)	2 (2.9)	0 (0.0)	1 (4.2)	–
H₂S concentration, nM	425.7±87.4	241.1±69.4	237.2±73.7	262.2±77.1	246.0±54.2	<0.001

Data are presented as n (%) for categorical data or mean±SD for continuous data. P values are for comparisons between controls and patients with aortic dissection. AVR/MVR indicates aortic valve replacement/mitral valve replacement; BMI, body mass index; CAD, coronary artery disease; and H_2S, hydrogen sulfide.

indicating that destruction of the endothelium may be a cause of the development of AAD.[10]

Posttranslational modification (PTM) of proteins allows cells to respond rapidly to environmental perturbations. Protein S-sulfhydration is a type of PTM that mainly occurs on thiols of reactive cysteine residues in response to redox stress.[11] Modification of reactive cysteine residues, which are important for protein functions, is involved in diverse biochemical functions.[12] For example, Jiang et al[13] found that S-sulfhydration of protein disulfide isomerase (PDI) at Cys53, Cys57, Cys397, and Cys 400 in 2 cysteine-terminal CXXC (Cys-Xaa-Xaa-Cys) domains enhanced its activity, alleviated hyperhomocysteinemia-induced endothelial endoplasmic reticulum (ER) stress, and attenuated development of atherosclerosis. Protein S-sulfhydration is generated by the transsulfuration pathway, which catabolizes cysteine and cystathionine to generate hydrogen sulfide (H_2S).[14] In the endothelium, cystathionine γ lyase (CSE) is the main enzyme that

accounts for the production of H_2S, and the CSE/H_2S system is important for endothelial homeostasis.[15] However, whether protein S-sulfhydration in the endothelium is involved in AAD remains unelucidated.

In this study, we found that the plasma H_2S concentration was lower in patients with aortic dissection (AoD) than in healthy controls. CSE levels were reduced in the endothelium of AAD mice and clinical AoD samples. S-sulfhydration of protein disulfide isomerase (PDI-SSH) is reduced in the ECs. The reduction of PDI-SSH at Cys343 and Cys400 impaired its reductase and substrate-binding activities, resulting in the activation of the protein kinase RNA-like endoplasmic reticulum kinase (PERK) signaling pathway and ER stress in the endothelium. At the mechanistic level, ZEB2 (zinc finger E-box binding homeobox 2) recruits the HDAC1-NuRD complex (histone deacetylase 1–nucleosome remodeling and deacetylase) to the promoter of *CTH* and inhibits its transcription. Inhibiting the formation of the HDAC1-ZEB2-NuRD complex restored
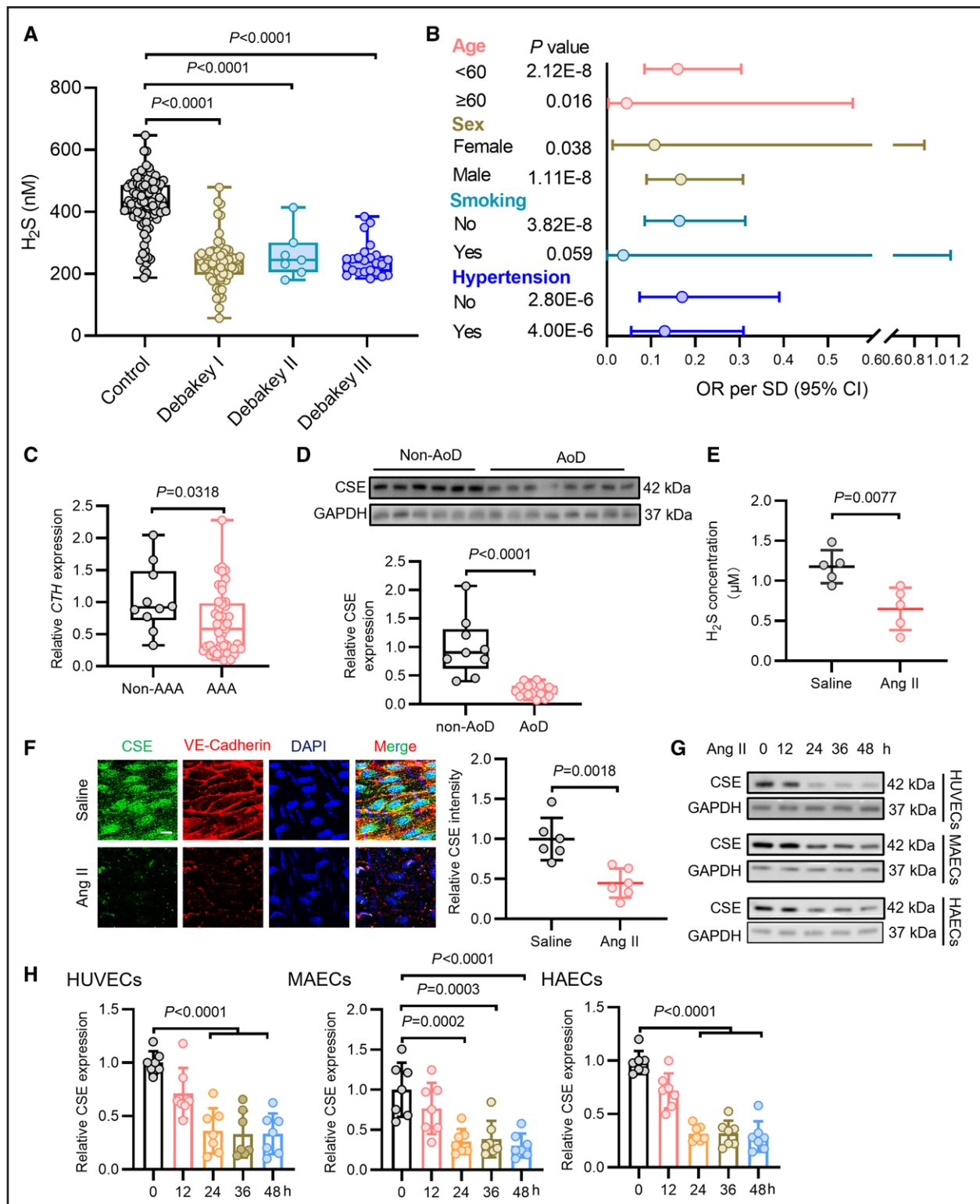
Figure 1. Dysfunction of the cystathionine γ lyase/hydrogen sulfide system in patients with aortic aneurysm and dissection and endothelium of aortic aneurysm and dissection mice.

A, Plasma levels of hydrogen sulfide (H_2S) in healthy controls (n=100) and **patients with aortic** dissection (AoD; n=99) with different disease status (68 DeBakey I, 7 DeBakey II, 24 DeBakey III). **B**, Forest plot showing the adjusted per-SD odds ratio (OR per SD) and 95% CI for plasma H_2S levels associated with AoD risk in subgroups. Binary logistic regression was adjusted for age, sex, smoking status, and history of hypertension. **C**, In silico analysis of *CTH* expression in aortic specimens of controls (non–abdominal aortic aneurysm [AAA]; n=10) and patients with AAA (n=49) on the basis of Gene Expression Omnibus data (accession code GSE57691); 2-tailed unpaired *t* test. **D**, Representative Western blotting and quantification of cystathionine γ lyase (CSE) expression in aortic specimens of controls (non-AoD; n=9) and patients with AoD (n=18); Mann-Whitney test. **E** and **F**, Eight-week-old male mice were infused with saline or (*Continued*)

Figure 1 Continued. angiotensin II (Ang II; 1000 ng/kg/min) for 28 days. **E**, The plasma levels of H$_2$S in saline-treated and Ang II–treated mice was determined (5 mice in each group); 2-tailed unpaired *t* test. **F**, En face staining of CSE in the endothelium of saline-treated and Ang II–treated mice (**right**, statistical results; scale bar=50 µm; 6 mice in each group); 2-tailed unpaired *t* test. **G** and **H**, Human umbilical vein endothelial cells (HUVECs), mouse aortic endothelial cells (MAECs), or human aortic endothelial cells (HAECs) were incubated with Ang II (10^{-6} M) for 12, 24, 36, or 48 hours, respectively. **G**, Representative Western blotting of CSE. **H**, quantification of CSE protein level (7 distinct samples for each group); ordinary 1-way ANOVA with Dunnett multiple comparisons test. **A** and **B**, Data presented as box-and-whisker plots, with 75th and 25th percentiles; bars represent maximal and minimal values. **C**, **D**, and **F**, Data represented as mean±SD. VE indicates vascular endothelial.

METHODS

[Expanded Methods](#) are available in the Supplemental Material. The data, methods, and study materials used to conduct the research are available from the corresponding authors on reasonable request. The mass spectrometry raw data have been deposited to the ProteomeXchange Consortium through the Proteomics Identification Database (https://www.ebi.ac.uk/pride/archive) partner repository with identifiers PXD038995, PXD038720, and PXD038715.

Study Population and Data Collection

The inclusion criteria were as follows: (1) patients with AoD >18 years of age; (2) obvious clinical manifestations of AoD, such as sudden onset of severe chest, back, or abdominal pain; and (3) false lumen or free intima detected using echocardiography, computed tomography angiography, magnetic resonance imaging, or aortic angiography. Patients with aortic trauma, pseudoaneurysm, or infectious diseases were excluded. Sex- and smoking-matched healthy controls who had no substantial systemic diseases, including ischemic heart disease, cancer, or infectious disease, were recruited from the Nanjing Drum Tower Hospital. The study was approved by the Ethics Committee of the Nanjing Drum Tower Hospital (2022-508-01) and informed consent was

obtained from all participants. A case–control study was established to compare serum H$_2$S levels of patients with AoD and healthy controls. A total of 99 patients with AoD and 100 healthy controls were recruited. Measures including sex, age, body mass index (BMI), hypertension, diabetes, smoking, and type of AoD were extracted from electronic medical records. Blood samples of patients with AoD were collected before surgery within 12 hours of admission. Blood samples from patients with AoD and healthy controls were collected; plasma was separated by centrifugation immediately and stored at −80℃ until use.

Human AoD and Non-AoD Samples

Human aortic tissue was collected in compliance with the Declaration of Helsinki. The presence of AoD was confirmed at the time of surgery by experienced cardiothoracic surgeons and the clinical phenotype diagnosis was confirmed using standard histopathology at the Second Affiliated Hospital of Nanjing Medical University. Dissected aortic aneurysmal tissue was collected during surgery from patients who had undergone aortic root and ascending aorta replacement or stent implantation of the descending aorta. The study was approved by the Ethics Committee of the Second Affiliated Hospital of Nanjing Medical University (2019KY094). All non-AoD samples used in this study were obtained from the Biospecimen Bank of the Nanjing First Hospital, Nanjing Medical University. The study was approved by the Ethics Committee of Nanjing First Hospital, Nanjing Medical University (approval KY20190404-03-KS-01). Patient information is summarized in Table S1.

Animal Studies

All animal experiments were conducted in accordance with the ARRIVE guidelines (Animal Research: Reporting of In Vivo

Table 2. Univariate and Multivariate Analyses of Risk Factors for Aortic Dissection Occurrence

Risk factors	Univariate logistic regression		Multivariate logistic regression	
	Odds ratio (95% CI)	*P* value	Odds ratio (95% CI)	*P* value
Age, y: ≥65 vs <65	1.03 (1.00–1.05)	0.017	0.98 (0.94–1.03)	0.566
Sex: male vs female	1.10 (0.499–2.053)	0.973	1.892 (0.522–6.859)	0.332
Smoking: smoker vs never smoked	0.633 (0.345–1.161)	0.139	1.088 (0.320–3.701)	0.892
BMI		0.070		
Overweight (25 to <30) vs normal or underweight (<25)	0.50 (0.27–0.90)	0.021	0.45 (0.14–1.45)	0.181
Obese (≥30) vs normal or underweight	0.71 (0.26–1.88)	0.493	0.57 (0.12–2.80)	0.488
Diabetes: yes vs no	0.558 (0.210–1.482)	0.242	0.304 (0.036–2.551)	0.273
Hypertension: yes vs no	7.99 (4.25–15.04)	<0.001	20.63 (5.47–77.80)	<0.001
H$_2$S	0.209 (0.143–0.305)	<0.001	0.16 (0.09–0.28)	<0.001

Multivariate logistic regression model. Adjusted for age, sex, body mass index (BMI), smoking, hypertension, and diabetes. H$_2$S indicates hydrogen sulfide.
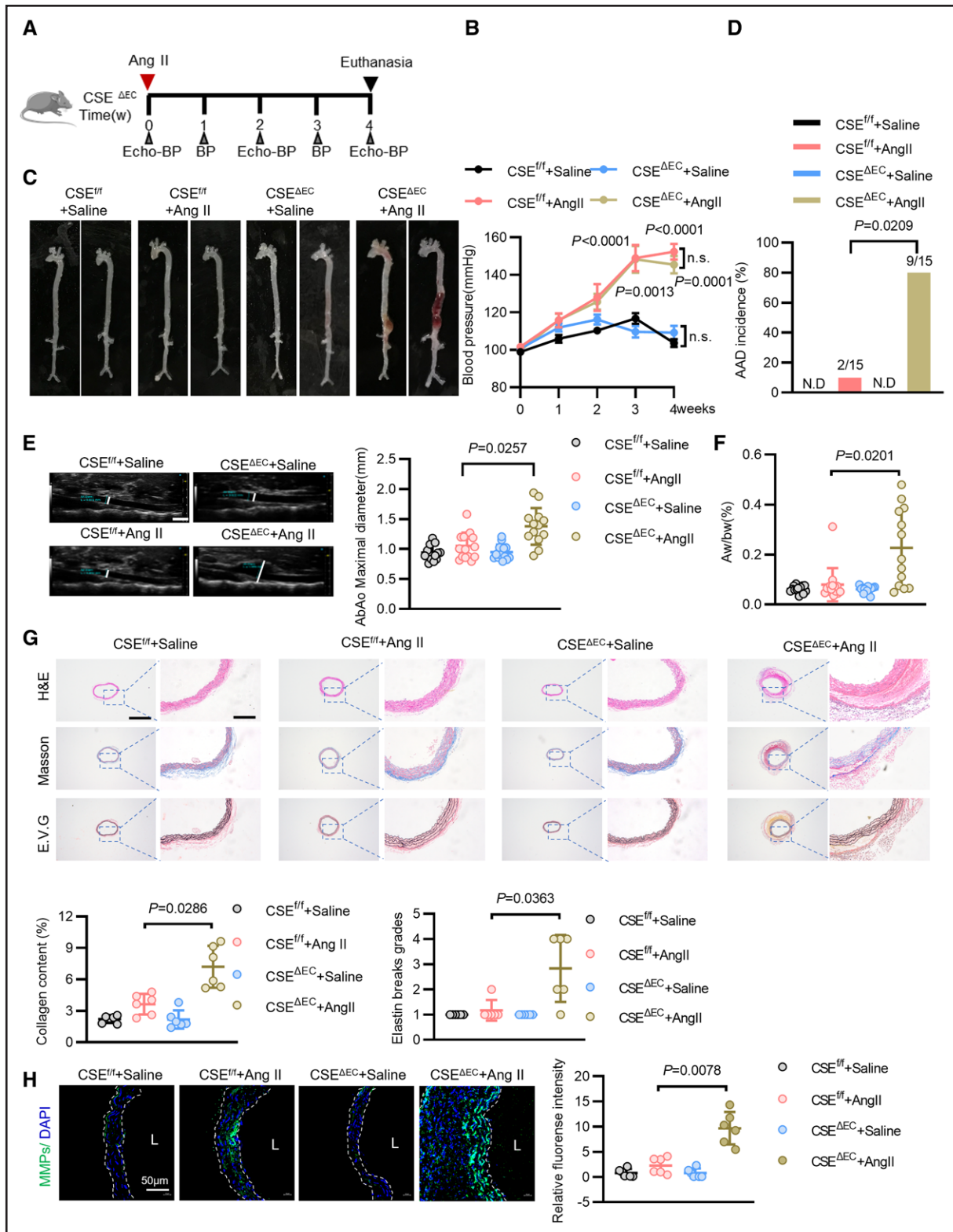
Figure 2. Deficiency of endothelial cystathionine γ lyase aggravates aortic aneurysm and dissection in vivo.
A, Experimental design. Eight-week-old cystathionine γ lyase (CSE)$^{flox/flox}$ (CSE$^{f/f}$) male mice or endothelium-specific CSE knockout (CSE$^{\Delta EC}$) mice were infused with saline or angiotensin II (Ang II; 1000 ng/kg/min) for 4 weeks, monitored for aortic dilation and blood pressure (echo-BP), and euthanized at the indicated time point. **B**, Systolic BP at 0, 1, 2, and 4 weeks; CSE$^{f/f}$+saline (n=10), CSE$^{f/f}$+Ang II (n=10), CSE$^{\Delta EC}$+saline (n=10), CSE$^{\Delta EC}$+Ang II (n=8–10); mixed-effects analysis followed by Tukey multiple comparisons test. **C**, Representative photograph of aortas in each group with Ang II or saline treatment for 28 days. **D**, Incidence of aortic aneurysm and dissection (AAD) for each group; Fisher exact test. **E**, Representative ultrasound images (**left**) and quantification of the maximal abdominal aorta (AbAo) diameters (**right**) *(Continued)*

Figure 2 Continued. from CSE^f/f+saline (n=15), CSE^f/f+Ang II (n=15), CSE^ΔEC+saline (n=15), and CSE^ΔEC+Ang II (n=13) mice; scale bar=1 mm. **F**, Statistical results of the ratio of aortic weight to body weight (Aw/bw) of CSE^f/f+saline (n=15), CSE^f/f+Ang II (n=15), CSE^ΔEC+saline (n=15), and CSE^ΔEC+Ang II (n=13) mice. **G**, Representative hematoxylin & eosin (H&E), Masson trichrome, and elastic van Gieson (EVG) staining of suprarenal AoAb sections (**bottom**, quantification of collagen content and grade of aortic elastic fiber fragmentation); scale bar=1 mm (**left**) and 100 μm (**right**); n=6 for each group. Collagen content was analyzed by Brown-Forsythe and Welch ANOVA followed by Dunnett T3 multiple comparisons test. Elastin break grades were analyzed by Kruskal-Wallis followed by Dunn multiple comparisons test. **H**, Representative immunofluorescence staining for matrix metalloproteinase (MMP) activity in the suprarenal abdominal aortas from differently treated mice; scale bar=50 μm (**right**, quantification of MMP fluorescence intensity); n=6 for each group. Brown-Forsythe and Welch ANOVA followed by Dunnett T3 multiple comparisons test. Data represented as mean±SD. EC indicates endothelial cell; L, lumen; ND, not detected; and ns, no significance.

Experiments) for the care and use of laboratory animals and protocols were approved by the Nanjing Medical University Animal Care and Use Committee (approval IACUC-1811016). HDAC1^flox/flox (HDAC1^f/f) mice were a gift from Professor Yunli Xie of Institutes of Brain Science, Fudan University. VE-Cadherin-Cre mice were a gift from Luyang Yu of Zhejiang University. Six-week-old male ApoE^−/− mice were purchased from the Animal Center of Nanjing University. CSE^flox/flox (CSE^f/f) mice containing loxP sites flanking exons 4 and 5 were constructed by Shanghai Model Organisms. Endothelial-specific CSE knockout (CSE^ΔEC) mice were generated by crossbreeding CSE^f/f mice with VE-Cadherin-Cre mice. Endothelial-specific HDAC1 knockout ApoE^−/− (HDAC1^ΔEC/ApoE^−/−) mice were generated by crossing HDAC1^f/f/ApoE^−/− mice with VE-Cadherin-Cre/ApoE^−/− mice. Only male mice were used in this study. Mice were kept under a 12-hour light/dark cycle at 23°C with ad libitum access to food and water.

Mouse AAD Model

For induction of the AAD model, 8-week-old mice were subcutaneously infused with Ang II (Sigma Aldrich; 1000 ng/kg/min) by a mini-pump (Alzet; model 2004) for 4 weeks. To determine the effect of GYY4137 or entinostat on AAD formation and progression, mice were intraperitoneally injected with entinostat solution (10 mg/kg/day) or GYY4137 (133 μM/kg/day) once daily from the time of Ang II infusion for 28 days; 0.9% sodium chloride was used as the vehicle.

Statistical Analysis

Data were analyzed using SPSS (version 26.0) and GraphPad Prism version 9.0.1 (GraphPad Software). Continuous variables were expressed as mean±SD or box-and-whisker plots, with 75th and 25th percentiles, when appropriate. Categorical variables were expressed as numbers and percentages. Comparisons between groups were performed using 2-sided t test, Mann-Whitney U test, or χ^2 test, as appropriate. Univariate and multivariate binary logistic regression were performed to evaluate the risk of H$_2$S and AoD incidence, with or without adjusting for clinical measures. The incidence of AoD was calculated across different BMI classes (BMI <25 kg/m^2, BMI 25 to <30 kg/m^2, BMI ≥30 kg/m^2). Odds ratios (ORs) and 95% CIs were also calculated. Differences among groups were evaluated using 1-way ANOVA followed by the Tukey or Dunnett test for post hoc comparisons when appropriate. Otherwise, the Kruskal-Wallis test followed by the Dunn multiple comparisons test was performed. Blood pressure was analyzed by mixed-effects analysis followed by the Tukey multiple comparisons test. Differences with $P<0.05$ was considered statistically significant.

Detailed materials and methods are presented in the Expanded Methods in the Supplemental Material.

RESULTS

Reduced Plasma H$_2$S Concentration in Patients With AoD

We first measured serum H$_2$S concentrations in patients with AoD and healthy controls. Data were collected from 199 individuals, including 99 patients with AoD (68 DeBakey I, 7 DeBakey II, and 24 DeBakey III) and 100 healthy controls. The demographic data and clinical characteristics are shown in Table 1. H$_2$S concentration was reduced in patients with AoD (DeBakey I, 237.2±73.7; DeBakey II, 262.2±77.1; DeBakey III, 246.0±54.2) compared with healthy controls (425.7±87.4 nM; $P<0.0001$; Figure 1A). Univariate and multivariate logistic regressions were then applied to evaluate the association between plasma H$_2$S levels and the incidence of AoD. We found that higher plasma H$_2$S levels were associated with lower odds of AoD (OR per SD, 0.16 [95% CI, 0.09–0.28]; $P<0.001$) after adjusting for common risk factors (age, sex, smoking, BMI, history of hypertension, and diabetes; see Table 2). The associations between plasma H$_2$S concentrations and AoD risks were consistent across the different subgroups defined by age, sex, smoking status, and history of hypertension (Figure 1B).

Reduced CSE Expression in the Endothelium Is Associated With the Occurrence of AAD

Analysis of the transcriptomic data (GSE57691) of the vascular tissues collected from healthy controls and patients with AAA showed reduced mRNA levels of *CTH* (Figure 1C). The expression of CSE was lower in the aorta of patients with AoD than in healthy controls; no difference in the expression level of cystathionine β-synthase (CBS) was observed (Figure S1A). Subcutaneous administration of Ang II by a mini pump was used to induce AAD in ApoE^−/− mice and the plasma concentrations of H$_2$S were reduced significantly in AAD mice (Figure 1E). En face staining confirmed that the expression of CSE was reduced in the vascular endothelium after Ang II administration (Figure 1F). In cultured human and mouse ECs, incubation with Ang II induced a time-dependent decrease in the mRNA and protein level
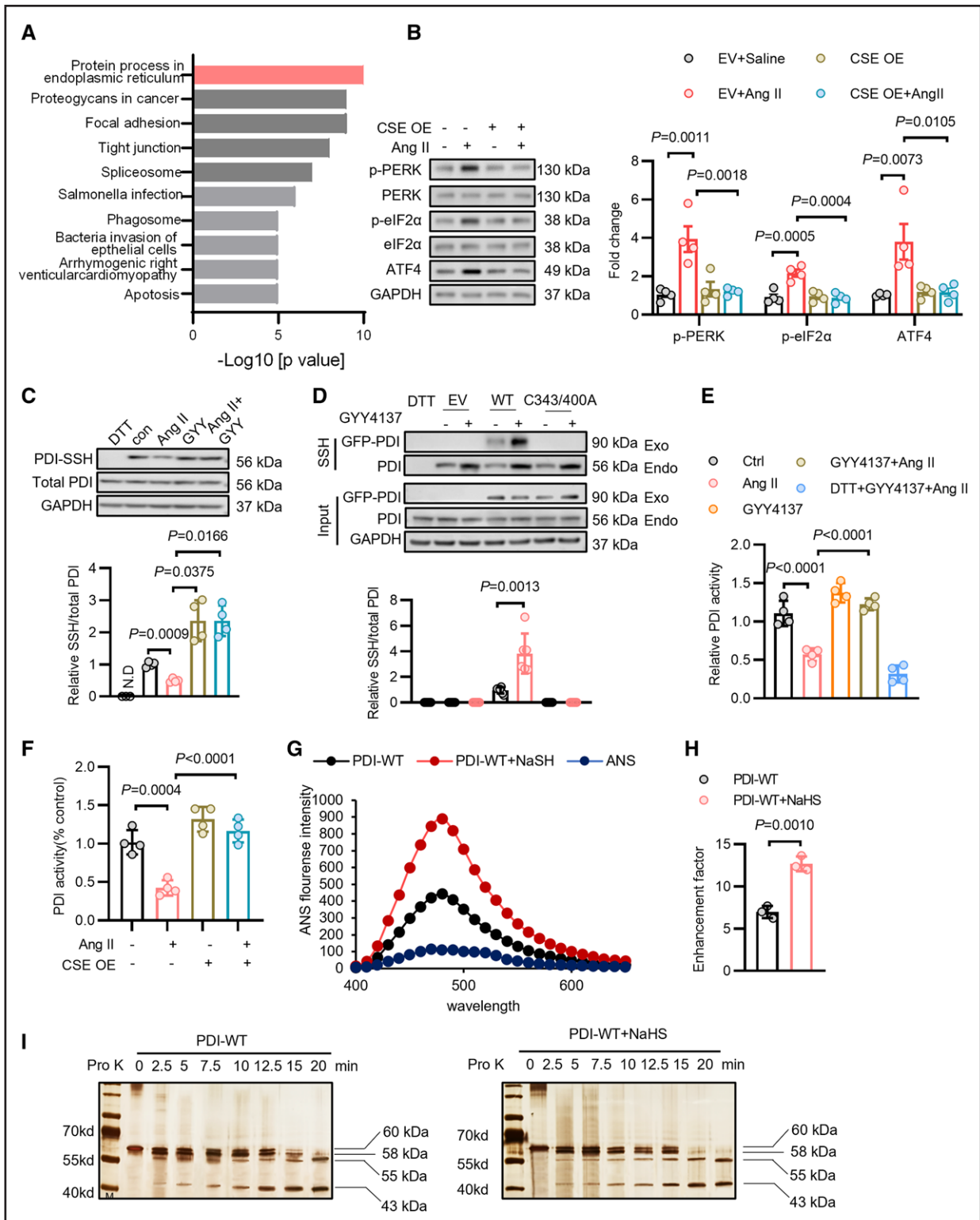
Figure 3. Reduction of protein disulfide isomerase S-sulfhydration in endothelium enhances endothelial endoplasmic reticulum stress.
A, KEGG (Kyoto Encyclopedia of Genes and Genomes) pathway enrichment analysis of persulfidated proteins in human umbilical vein endothelial cells (HUVECs) stimulated with angiotensin II (Ang II) and GYY4137 (100 μM; 24 hours). **B**, Representative Western blotting (**left**) and quantification of the protein kinase RNA-like endoplasmic reticulum kinase (PERK) signaling pathway protein levels (**right**) in Ang II–treated HUVECs transfected with cystathionine γ lyase (CSE) overexpression (OE) vectors; 4 independent experiments; ordinary 1-way ANOVA followed by Tukey multiple comparisons test. **C**, Representative modified biotin-switch analysis (**top**) and quantification (**bottom**) of S-sulfhydration of protein disulfide isomerase (PDI-SSH) in Ang II–treated HUVECs incubated with or without GYY4137 (100 μM; 24 hours); 4 independent experiments; Brown-Forsythe and Welch ANOVA followed by Dunnett T3 multiple comparisons test. (*Continued*)

Figure 3 Continued. D, Modified biotin-switch analysis detecting S-sulfhydration of green fluorescent protein (GFP)–protein disulfide isomerase (PDI) after GYY4137 (100 µM, 24 hours) incubation in HUVECs transfected with vectors encoding GFP (EV), GFP-tagged PDI–wild-type (WT), or GFP-tagged PDI mutant (C343/400A); 6 independent experiments; unpaired *t* test. **E**, Reductase activity of PDI in Ang II–stimulated HUVECs with or without GYY4137 (100 µM; 24 hours) treatment; 4 independent experiments; ordinary 1-way ANOVA followed by Tukey multiple comparisons test. **F**, Reductase activity of PDI in Ang II–stimulated HUVECs transfected CSE overexpression vector (CSE OE); 4 independent experiments; ordinary 1-way ANOVA followed by Tukey multiple comparisons test. **G**, 1-anilinonaphthalene-8-sulfonic acid (ANS) fluorescence spectra of PDI-WT protein incubated with or without NaSH (100 µM; 50 minutes) and quantification of enhancement factor (**H**); 3 independent experiments; unpaired *t* test. **I**, Representative limited proteolysis analysis of PDI WT and PDI WT+NaSH (100 µM; 50 minutes) incubated by proteinase K (Pro K) for indicated time points; 2 in each group; data presented as mean±SD. ATF4 indicates activating transcription factor 4; AU, arbitrary units; DTT, dithiothreitol; eIF2α, eukaryotic translation initiation factor 2A; p-eIF2α, phospho–eukaryotic translation initiation factor 2A; and p-PERK, phospho–protein kinase RNA-like endoplasmic reticulum kinase.

of CSE (Figure 1G and 1H and Figure S1B) and the concentration of H_2S declined in the cultural medium (Figure S1C). Cyclic mechanical stretch mimicked the increased vascular wall stress during AAD; the expression of CSE was also reduced in human umbilical vein ECs (HUVECs) stimulated with cyclic mechanical stretch (Figure S1D). We also compared the expression levels of CSE in the endothelial and smooth muscle cells and found a higher level of CSE in the ECs. Ang II treatment did not affect CSE protein levels in the smooth muscle cells, implying an important role of endothelial CSE in AAD (Figure S1E).

EC-Specific CSE Knockout Aggravates Ang II–Induced AAD in Mice

To determine the role of endothelial CSE in the progression of AAD, we constructed $CSE^{\Delta EC}$ mice by crossing $CSE^{f/f}$ with VE-Cadherin-Cre mice. We then induced AAD in mice by subcutaneous infusion of Ang II for 4 weeks (Figure 2A). Western blotting confirmed the deletion of CSE in ECs isolated from $CSE^{\Delta EC}$ mice (Figure S2A). En face staining further revealed a lack of CSE expression in the endothelium of the $CSE^{\Delta EC}$ mice (Figure S2B). It has been reported that systemic knockout of CSE in mice increases systolic blood pressure (SBP). Thus, we monitored the SBP of $CSE^{f/f}$ and $CSE^{\Delta EC}$ mice from 6 to 50 weeks, and no difference in SBP between the 2 genotypes was observed (Figure S2C). Ang II treatment increased SBP in both genotypes (Figure 2B). Ang II treatment induced AAAs or lethal AoD in only 2 of the 15 $CSE^{f/f}$ mice, similar to a previous report,[16] whereas Ang II treatment triggered AAD in 9 of the 15 $CSE^{\Delta EC}$ mice (Figure 2C and 2D). According to ultrasound imaging, $CSE^{\Delta EC}$+Ang II mice exhibited a significant increase in abdominal aortic diameter compared with $CSE^{f/f}$+Ang II mice (1.38±0.10 versus 1.05±0.07 mm; *P*=0.026; Figure 2E). The diameter of thoracic aorta, ascending aorta, descending aorta, and transaortic arch were comparable among 4 groups (Figure S2D and S2G). Ang II infusion induced larger maximal outer suprarenal aortic diameter in the $CSE^{\Delta EC}$ mice than in the $CSE^{f/f}$ mice (Figure S2H). The ratio of aortic to body weight was significantly higher in the $CSE^{\Delta EC}$+Ang II mice than in the $CSE^{f/f}$+Ang II mice (Figure 2F). Hematoxylin & eosin staining revealed a significant increase in the aortic medial thickness. Masson

trichrome staining revealed increased deposition of collagen and elastic van Gieson staining showed more severe fragmentation of elastic fibers in the $CSE^{\Delta EC}$+Ang II mice (Figure 2G). Moreover, we found that the activity of matrix metalloproteinase increased significantly in the suprarenal aortas of the $CSE^{\Delta EC}$ mice by in situ zymography (Figure 2H). These results demonstrate that the knockout of endothelial CSE exacerbates the development of AAD.

Reduction of PDI-SSH in Endothelium Enhanced Endothelial ER Stress

S-sulfhydration of reactive cysteines is a reversible post-translational modification mediated by H_2S, which regulates protein functions. We attempted to identify the persulfidated proteins in the ECs during AAD. A modified biotin switch combined with a liquid chromatography–mass spectrometry assay revealed reduced protein S-sulfhydration in Ang II–treated HUVECs, which was reversed by pretreatment with the H_2S donor GYY4137 (Figure S3A). KEGG (Kyoto Encyclopedia of Genes and Genomes) pathway enrichment analysis showed that persulfidated proteins were enriched in protein processing in the ER pathway (Figure 3A). Gene set enrichment analysis of the transcriptome data of AoD and normal human aorta (GSE147026) identified that genes involved in protein processing in the ER showed increased expression in the aorta of patients with AoD (Figure S3B). These findings indicate that ER stress might be implicated in endothelial dysfunction during AAD. ATF6 (activated transcription factor 6), PERK, and IRE1 (inositol-requiring 1) are endogenous ER stress sensors.[17] We examined the activation of these proteins in the HUVECs. Ang II treatment did not affect the phosphorylation of IRE1a or expression of ATF6 (Figure S3C). In contrast, the PERK signaling pathway was activated, manifested as increases in the phosphorylation of PERK (p-PERK) and eIF2a (eukaryotic initiation factor 2a; p-eIF2a) and the expression of ATF4 after Ang II treatment. Overexpression of CSE significantly inhibited the activity of the PERK signaling pathway (Figure 3B).

We then analyzed the hub genes involved in ER stress. Common persulfidated proteins were collected in 2 repeated assays. The common targets were further overlapped with proteins interacting with CSE, as
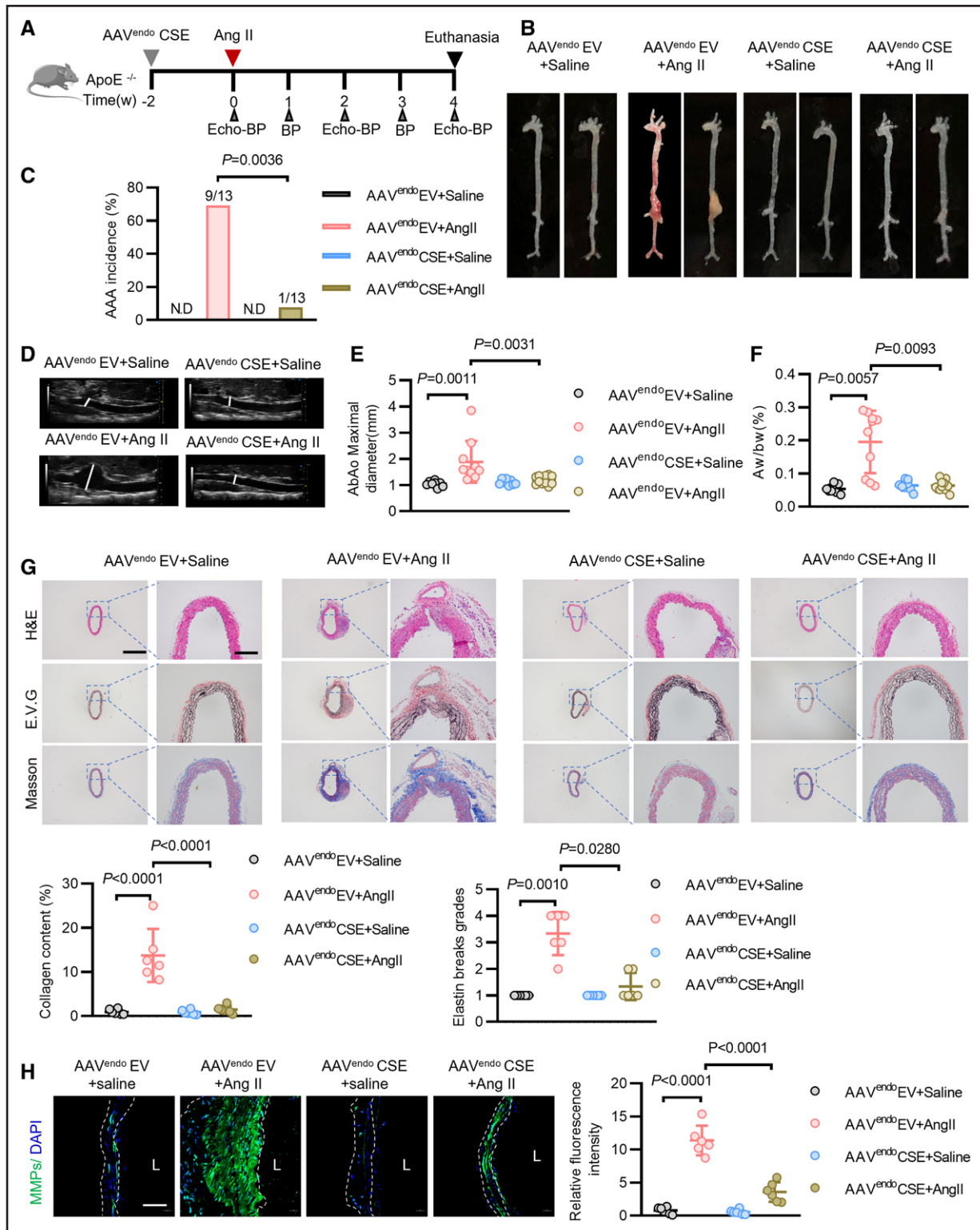
Figure 4. Overexpression of cystathionine γ lyase in endothelium alleviates aortic aneurysm and dissection by regulating protein disulfide isomerase S-sulfhydration and endoplasmic reticulum stress.

A, Experimental design. Six-week-old *APOE*−/− mice were intravenously injected with the endothelial cell (EC)–enhanced adeno-associated virus (AAV) vector encoding either green fluorescent protein (GFP; AAVendoEV) or cystathionine γ lyase (CSE; AAVendoCSE). Two weeks later, mice were infused with saline or angiotensin II (Ang II; 1000 ng/kg/min) for another 4 weeks, monitored for aortic dilation and blood pressure (echo-BP), and euthanized at the indicated time point. **B**, Representative photographs of aortas in each group with Ang II treatment for 28 days. **C**, Incidence of aortic aneurysm and dissection for each group; Fisher exact test. **D**, Representative ultrasound images and quantification of the maximal abdominal aorta (AbAo; **E**) diameters of AAVendo EV+saline (n=8), AAVendoEV+Ang II (n=10), AAVendoCSE+saline (n=8), and (*Continued*)
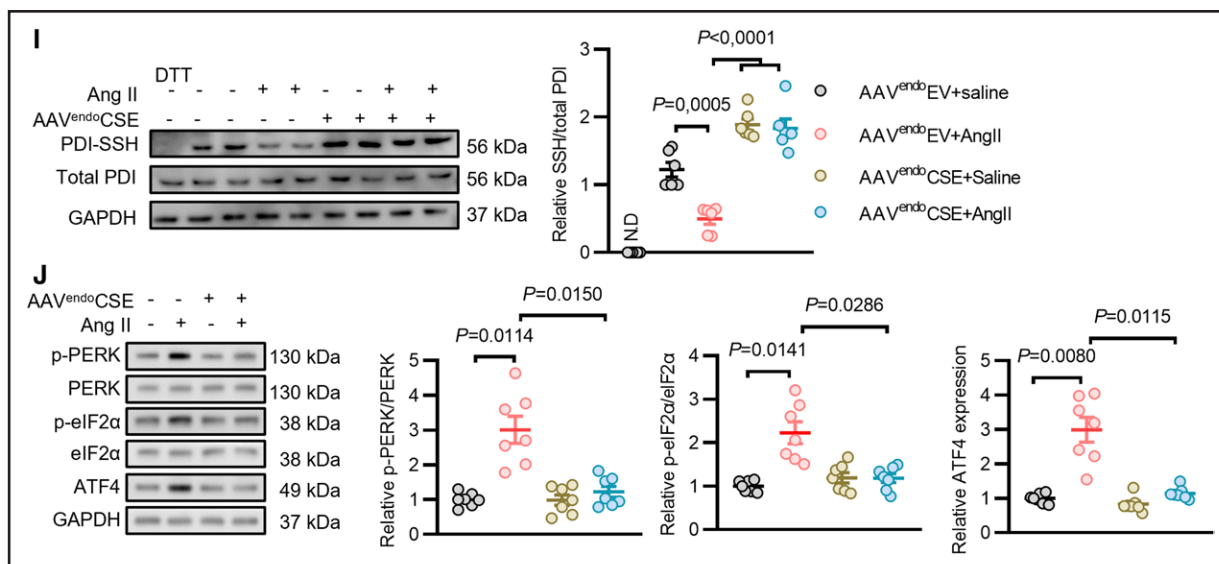
Figure 4 Continued. AAV^endoCSE+Ang II mice (n=12); scale bar=1 mm; ordinary 1-way ANOVA with Tukey multiple comparisons test. **F**, Statistical results of the ratio of aortic weight to body weight (Aw/bw) of AAV^endo EV+saline (n=8), AAV^endoEV+Ang II (n=10), AAV^endoCSE+saline (n=8), and AAV^endoCSE+Ang II mice (n=12); Brown-Forsythe and Welch ANOVA followed by Tamhane T2 multiple comparisons test. **G**, Representative hematoxylin & eosin (H&E), Masson trichrome, and elastic van Gieson (EVG) staining of suprarenal AoAb sections. **Bottom** shows the quantification of collagen content and grade of aortic elastic fiber fragmentation; scale bar=1 mm (**left**) and 100 μm (**right**); 6 in each group; collagen content, ordinary 1-way ANOVA with Tukey multiple comparisons test; elastin break grades, Kruskal-Wallis followed by Dunn multiple comparisons test. **H**, Representative immunofluorescence staining for matrix metalloproteinase (MMP) activity in the suprarenal abdominal aortas from differently treated mice; scale bar=50 μm. **Right**, the quantification of MMP fluorescence intensity; 6 in each group; ordinary 1-way ANOVA with Tukey multiple comparisons test. **I**, Representative modified biotin-switch analysis (**top**) and quantification (**bottom**) of S-sulfhydration (SSH) of protein disulfide isomerase (PDI) in aortas from AAV^endoEV+saline, AAV^endoEV+Ang II, AAV^endoCSE+saline, and AAV^endoEV+Ang II mice; 6 distinct samples for each group; ordinary 1-way ANOVA followed by Tukey multiple comparisons test. **J**, Representative Western blotting (**left**) and quantification of protein levels in protein kinase RNA-like endoplasmic reticulum kinase (PERK) signaling pathway (**right**) in aortas from AAV^endoEV+saline, AAV^endoEV+Ang II, AAV^endoCSE+saline, and AAV^endoEV+Ang II mice; 7 distinct samples for each group; ordinary 1-way ANOVA followed by Tukey multiple comparisons test for phospho−PERK (p-PERK)/PERK; Brown-Forsythe and Welch ANOVA followed by Tamhane T2 multiple comparisons test for phospho−eukaryotic translation initiation factor 2A(p-eIF2α)/eukaryotic translation initiation factor 2A (eIF2α) and activating transcription factor 4 (ATF4). Data presented as mean±SD. DTT indicates dithiothreitol; L, lumen; and ND, not detected.

reported by Bibli et al,[17] first 127 overlapping proteins were identified among the 3 datasets (Figure S3D), including RNA binding protein human antigen R, as previously reported.[17] A protein−protein interaction network of these proteins was constructed using the STRING database; the network was then imported into Cytoscape software and core genes were identified using CytoHubba. The top 10 genes were screened, of which the top scoring gene was *P4HB* (Figure S3E). *P4HB* encodes PDI, which catalyzes protein folding and maturation.[18] The modified biotin switch assay confirmed that Ang II reduced PDI-SSH, and GYY4137 pretreatment restored the level of PDI-SSH (Figure 3C). We then sought to identify the cysteine residues undergoing PDI modification. PDI has 6 cysteine residues that can potentially be persulfidated. Site-directed mutagenesis revealed that Cys343 and Cys400 were modified (Figure S3F). To confirm this observation, we transfected HUVECs with plasmids containing green fluorescent protein (GFP), GFP-PDI wild-type (WT), or GFP-PDI C343/400A; incubated them with GYY4137; and determined the level of PDI-SSH. We found a significant increase in the level of PDI-SSH in HUVECs

transfected with GFP-PDI-WT upon incubation with GYY4137, but no exogenous PDI-SSH was observed in cells overexpressing GFP-PDI C343/400A (Figure 3D). These observations confirmed that S-sulfhydration occurs on Cys343 and Cys400 in PDI.

The structure of PDI is a-b-b′-x-a′, where a and a′ represent the thioredoxin-like domains that mediate disulfide bond shuffling and b and b′ are substrate binding domains.[19] Cys400 resides in the a′ domain of PDI and Cys343 resides in the b′ domain, indicating that PDI-SSH might influence its catalytic and substrate binding activity. Using a dieosin-diglutathione assay,[20] we found that Ang II treatment reduced the reductase activity of PDI, which could be restored by GYY4137 (Figure 3E). The application of dithiothreitol to abolish S-sulfhydration could further lower the reductase activity of PDI, confirming that the reductase activity of PDI can be regulated by S-sulfhydration (Figure 3E). In line with these observations, overexpression of CSE restored the reduction in PDI reductase activity in HUVECs stimulated with Ang II (Figure 3F).

There is a continuous hydrophobic surface on the inner side of the active PDI, which mediates its
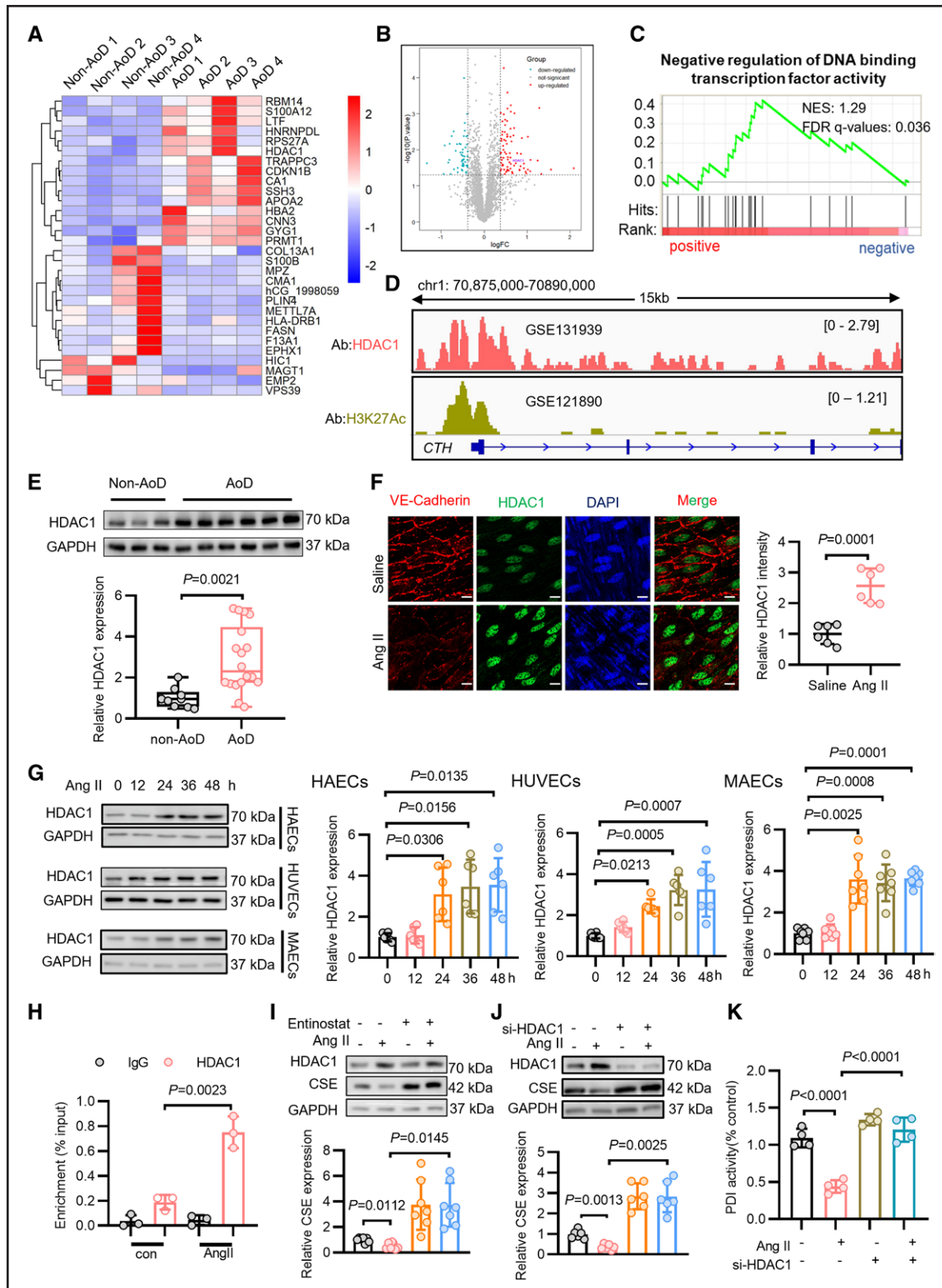
Figure 5. The level of HDAC1 expression increases during the development of aortic aneurysm and dissection.
A, Heatmap of differentially expressed proteins in aortic specimens of controls (non–aortic dissection [AoD]; n=4) and patients with AoD (n=4). Various color intensities indicate the expression levels. **Bottom** expressions are shown by blue and **top** by red. **B**, Volcano plot of gene expression change (log2 of fold change [FC]; x axis) and statistic fluorescence significance of this change (−log10 of P value; y axis) in a comparison of non-AoD with AoD. **C**, Gene set enrichment (GSE) analysis for differentially expressed genes. **D**, Recruitment of HDAC1 (histone deacetylase 1) and H3K27Ac (acetylated H3K4) to cystathionine γ lyase (*CSE*) on the basis of in silica analysis of chromatin immunoprecipitation followed by sequencing data (accession code GSE131939 for HDAC1 and GSE121890 for H3K27Ac). **E**, Representative Western blotting *(Continued)*

Figure 5 Continued. and quantification of HDAC1 expression in aortic specimens of controls (non-AoD; n=9) and patients with AoD (n=18). Data are presented as box-and-whisker plots, with 75th and 25th percentiles; bars represent maximal and minimal values; Mann-Whitney test. **F**, Representative image and statistical analysis of en face fluorescent staining of HDAC1 in vascular endothelium of mice treated with saline or angiotensin II; scale bar=50 μM; 6 mice per group; unpaired *t* test. **G**, Representative Western blotting and quantification of CSE protein levels; 6 independent experiments for human umbilical vein endothelial cells (HUVECs) and human aortic endothelial cells (HAECs) and 7 independent experiments for mouse aortic endothelial cells (MAECs); Brown-Forsythe and Welch ANOVA followed by Dunnett T3 multiple comparisons test of HDAC1 in HAECs and MAECs; Kruskal-Wallis followed by Dunn multiple comparisons test of HDAC1 in HUVECs. **H**, Chromatin immunoprecipitation assay for HDAC1 enrichment to the *CTH* promoter; samples were prepared from HUVECs exposed in PBS (control) or Ang II (10^{-6} M; 24 hours). Immunoglobulin G immunoprecipitation was used as control; 3 independent experiments; unpaired *t* test. **I**, Western blotting analyses of the expression of CSE in Ang II–treated HUVECs pretreated with the HDAC1 inhibitor entinostat (10 μM; 12 hours) or PBS; 7 independent experiments per group; Brown-Forsythe and Welch ANOVA followed by Tamhane T2 multiple comparisons test. **J** and **K**, HUVECs were transfected with siNC or si-HDAC1, followed by stimulation with Ang II and the level of CSE ((**J**; n=6) and the activity of protein disulfide isomerase (**K**; PDI; n=4) was determined. **J**, Brown-Forsythe and Welch ANOVA followed by Tamhane T2 multiple comparisons test. **K**, Ordinary 1-way ANOVA followed by Tukey multiple comparisons test. Data presented as mean±SD. FDR indicates false discovery rate; and NES, normalized enrichment score.

substrate-binding activity. This hydrophobic surface can be probed by ANS (1-anilinonaphthalene-8-sulfonic acid) by detecting the fluorescence intensity.[21] We purified recombinant PDI, incubated it with NaHS or PBS, and detected the substrate-binding activity of PDI using ANS. NaHS incubation increased the fluorescence intensity, indicating an increase in the substrate binding activity of PDI (Figure 3G and 3H). Furthermore, it has been reported that an open conformation of PDI, which is more sensitive to proteinase K digestion, is critical for its substrate binding activity.[21] In a limited proteolysis assay, PDI incubated with NaHS was digested more rapidly with proteinase K, indicating a more open conformation (Figure 3I). These data confirm that the S-sulfhydration of PDI increases its activity. On the basis of these findings, we proposed that the activity of PDI was increased by S-sulfhydration, and Ang II treatment reduced PDI activity by reducing its S-sulfhydration.

Overexpression of CSE in Endothelium Increased PDI-SSH and Alleviated AAD

We then used the EC-enhanced adeno-associated virus (AAV)[22] expressing HA (human influenza hemagglutinin)–CSE (AAV^endo^-CSE) to increase CSE levels in the endothelium of ApoE^−/−^ mice. ApoE^−/−^ mice transfected with an AAV vector containing GFP (AAV^endo^-EV) were used as controls. The experimental protocol is shown in Figure 4A. Western blot analysis of the HA tag confirmed increased expression of CSE in the aorta of AAV^endo^-CSE mice (Figure S4A). En face staining revealed increased CSE levels in the endothelium of AAV^endo^-CSE mice, with or without Ang II infusion (Figure S4B). Ang II infusion led to a comparable increase in SBP in AAV^endo^-CSE and AAV^endo^-EV mice (Figure S4C). Ang II treatment induced AAAs or lethal aortic dissections in AAV^endo^-EV mice, whereas overexpression of CSE in the endothelium reduced the incidence of AAD (AAV^endo^-EV+Ang II, 9/13; AAV^endo^-CSE+Ang II, 1/13; Figure 4B and 4C). The maximal abdominal aortic diameter and aortic weight/body weight in the AAV^endo^-CSE+Ang II mice were significantly reduced compared with those in the AAV^endo^-EV+Ang

II mice (Figure 4E and 4F). The diameters of the ascending aorta, thoracic aorta, descending aorta, and transaortic arch were comparable among the 4 groups (Figure S4D through S4G). Moreover, Ang-II–infused AAV^endo^-EV mice showed a larger maximal external diameter of the suprarenal aorta than the saline-infused mice, which was significantly reduced in AAV^endo^-CSE mice (Figure S4H). The increase in aortic medial thickness, fragmentation of elastic fibers, deposition of collagen, and activity of matrix metalloproteinases were inhibited by overexpression of CSE in the endothelium (Figure 4G and 4H). PDI-SSH was reduced in the aorta of AAD mice and EC-specific overexpression of CSE restored its levels (Figure 4I). Activation of the PERK signaling pathway in the aorta of AAD mice was alleviated by EC-specific overexpression of CSE (AAV^endo^-CSE; Figure 4J). These observations collectively indicate a protective role of endothelial CSE by regulating PDI-SSH and ER stress in the progression of AAD.

ZEB2 Recruits HDAC1-NuRD Complex to Repress CSE Transcription

After confirming the involvement of endothelial CSE in the regulation of PDI-SSH during AAD, we investigated the upstream factors that reduce the expression of CSE. We performed an unbiased proteomic screening of aortic samples from 4 patients with AoD and 4 healthy controls (non-AoD). Overall, 317 proteins were differentially expressed (false discovery rate *q* value<0.05, fold change >1.2 or <1/1.2), including 193 upregulated and 124 downregulated proteins (Figure 5A and 5B). We performed gene set enrichment analysis and found that genes associated with negative regulation of the DNA-binding transcription factor activity pathway were enriched (Figure 5C), in which HDAC1 showed the highest fold change. In silico analysis of the chromatin immunoprecipitation followed by sequencing data of HDAC1 and H3K27Ac (acetylated H3K4) from available data sets (GSE131939, GSE121890) showed the recruitment of HDAC1 and H3K27Ac to the promoter region of *CTH* (Figure 5D). The H3K27Ac level decreased in HUVECs
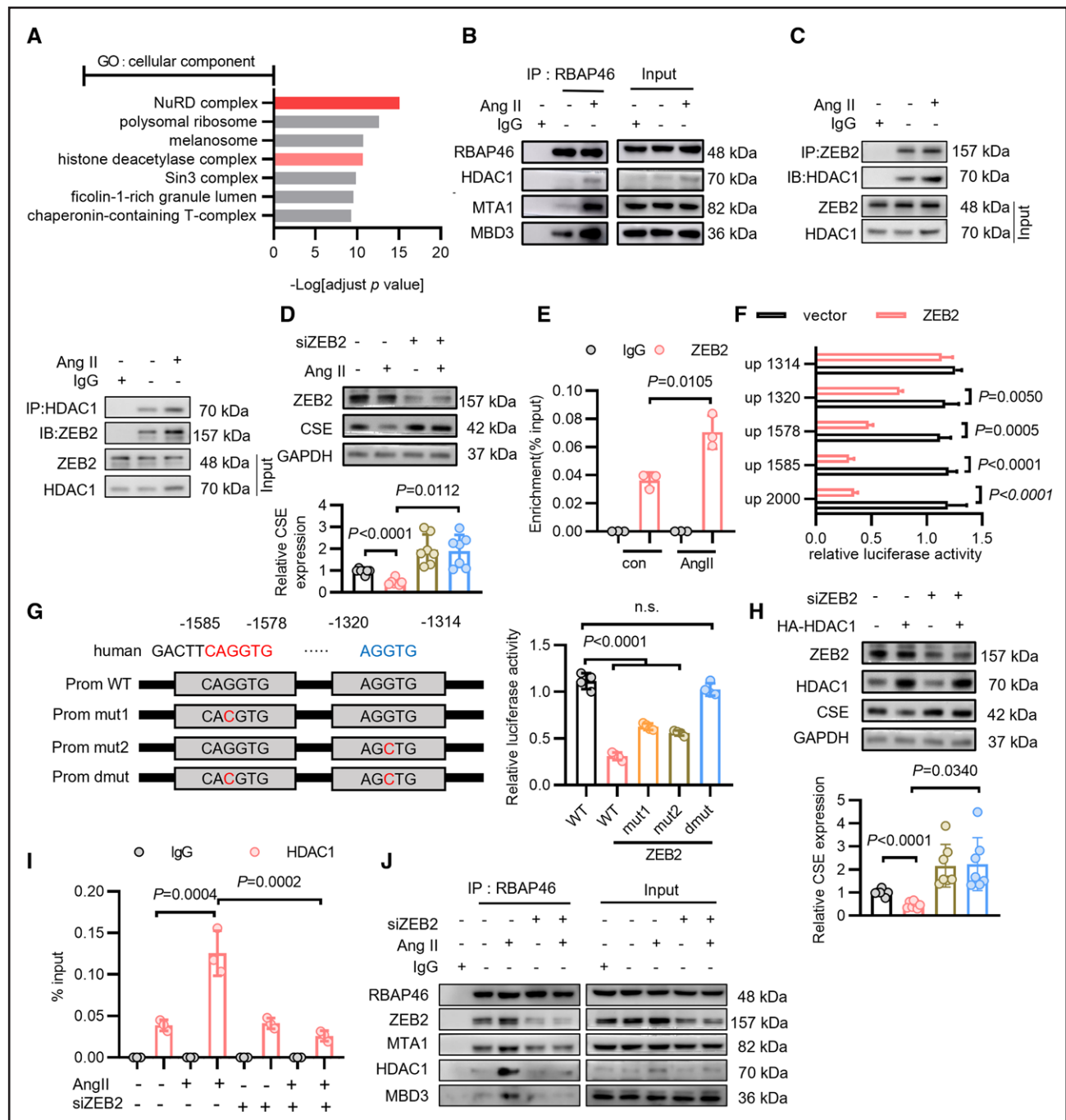
Figure 6. ZEB2 recruits HDAC1-NuRD complex to repress cystathionine γ lyase expression.
A, Gene Ontology (GO) categories of proteins that can interact with HDAC1 (histone deacetylase 1; −log10 of adjust *P* value; *x* axis) and cellular components of these proteins (GO: cellular component; *y* axis). **B**, The formation of the HDAC1−NuRD (nucleosome remodeling and deacetylase) complex detected by coimmunoprecipitation assay. Human umbilical vein endothelial cells (HUVECs) were challenged with PBS or angiotensin II (Ang II; 10^{-6}; 24 hours) and the cell lysates were immunoprecipitated with anti-RBAP46 (histone-binding protein RBBP7) or immunoglobulin G (IgG) and immunoblotted with the indicated antibodies; 3 independent experiments. **C**, The interaction of HDAC1 with ZEB2 (zinc finger E-box-binding homeobox 2) assessed by coimmunoprecipitation assay. HUVECs were challenged with PBS or Ang II (10^{-6}; 24 hours) and the cell lysates were immunoprecipitated with anti-ZEB2, anti-HDAC1, or anti-IgG antibodies and immunoblotted with the indicated antibodies; 3 independent experiments. **D**, Western blotting analysis of the expression of cystathionine γ lyase (CSE) in Ang II–treated HUVECs transfected with siNC or si-ZEB2; 7 independent experiments; Brown-Forsythe and Welch ANOVA followed by Tamhane T2 multiple comparisons test. **E**, Chromatin immunoprecipitation assays for HDAC1 enrichment to the *CTH* promoter on chromatin prepared from HUVECs exposed to PBS (control) or Ang II (10^{-6} M; 24 hours). IgG immunoprecipitation was used as control; 3 independent experiments; 2-tailed unpaired *t* test. **F**, Luciferase reporter constructs with the truncated (−1585, −1578, −1320, and −1314) and full-length *CTH* promoter were cotransfected with a ZEB2 coding vector or empty vector (vector) into HEK293T cells, and luciferase activity was evaluated; 3 independent experiments per group; 2-tailed unpaired *t* test. **G**, Diagram of luciferase reporter constructs containing the wild-type *(Continued)*

Figure 6 Continued. (prom WT) *CTH* promoter or promoters with mutations at ZEB2 binding motifs (prom mut1, prom mut2, and prom dmut; **left**) and the relative luciferase activity (**right**); 4 independent experiments per group; ordinary 1-way ANOVA with Tukey multiple comparisons test. **H**, HUVECs were transfected with vectors coding for HA-HDAC1 and then transfected with siZEB2 or siNC. CSE was detected by Western blotting (**top**) and the level of CSE was determined in 7 independent experiments (**bottom**); Brown-Forsythe and Welch ANOVA followed by Dunnett T3 multiple comparisons test. **I**, HUVECs were transfected with siZEB2 and then incubated with Ang II; the enrichment of HDAC1 to *CTH* promoter was determined by chromatin immunoprecipitation PCR; 3 independent experiments; ordinary 1-way ANOVA with Tukey multiple comparisons test. **J**, HUVECs were transfected with siZEB2 followed by incubation with Ang II, and the cell lysates were immunoprecipitated with anti-RBAP46 and IgG; the formation of HDAC1-NuRD complex was determined by coimmunoprecipitation; 3 independent experiments. Data represented as mean±SD. MBD3 indicates methyl-CpG-binding domain protein 3; and MTA1, metastasis-associated protein 1.

stimulated with Ang II in a dose-dependent manner (Figure S5A). In accordance with the proteomics data, Western blotting confirmed an increase in the protein level of HDAC1 in the aorta of patients with AoD (Figure 5E). En face staining showed increased expression of HDAC1 in endothelium of AAD mice (Figure 5F). In cultured human and mouse aortic ECs, Ang II treatment induced a time-dependent increase in HDAC1 protein levels (Figure 5G), whereas the protein levels of other class I histone deacetylases, including HDAC2 and HDAC3, were not affected by Ang II (Figure S5B and S5C). Furthermore, we observed a higher protein level of HDAC1 in human aortic endothelial cells than in human aortic smooth muscle cells, and the expression of HDAC1 increased significantly in human aortic endothelial cells rather than in human aortic smooth muscle cells upon Ang II treatment (Figure S5D). Next, we performed a chromatin immunoprecipitation assay and confirmed that Ang II could increase the binding of HDAC1 to the *CTH* promoter region (Figure 5H). Entinostat, a class I HDAC inhibitor with higher selectivity for HDAC1, increased the protein level of CSE in HUVECs (Figure 5I). Knockdown of HDAC1 significantly increased the protein level of CSE in HUVECs (Figure 5J), restored the activity of PDI (Figure 5K), and alleviated activation of the PERK signaling pathway (Figure S5E).

To further elucidate the mechanism underlying the recruitment of HDAC1 to the *CTH* promoter, coimmunoprecipitation combined with mass spectrometry analysis was conducted to identify proteins interacting with HDAC1 (Figure S5F). A total of 301 proteins were identified to interact with HDAC1 and Gene Ontology analysis showed enrichment of multiple components of the histone deacetylase complex, including the NuRD complex (Figure 6A). Coimmunoprecipitation verified the formation of the endogenous HDAC1-NuRD complex in HUVECs stimulated with Ang II (Figure 6B). We further evaluated the transcription factors required for the formation of the HDAC1-NuRD complex. A protein–protein interaction network of HDAC1 interacting proteins was constructed using the STRING database and ZEB2 was identified as a transcriptional factor that could interact with HDAC1 (Figure S5G). Coimmunoprecipitation confirmed the interaction between endogenous ZEB2 and HDAC1 (Figure 6C). Knockdown of ZEB2 rescued Ang II–induced dysregulation of CSE (Figure 6D). Furthermore, chromatin immunoprecipitation assay verified the binding of ZEB2 to the promoter of *CTH* and Ang II increased this binding (Figure 6E). The 2.0-kb human *CTH* promoter region contains 2 ZEB2 binding motifs (−1585 to −1578; −1320 to −1314). Next, we constructed a series of luciferase reporter plasmids containing truncated *CTH* promoter sequences and investigated the effects of ZEB2 on luciferase activity. ZEB2 overexpression significantly reduced the luciferase activity of these constructs (ie, −1320, −1578, −1585, and −2000; Figure 6F). We then constructed *CTH* promoters containing WT (prom WT), single mutation (prom mut1 and prom mut2), and double mutations (prom dmut) of the ZEB2-binding motifs (Figure 6G, left). We found that overexpression of ZEB2 reduced the luciferase activity of prom WT, prom mut1, and prom mut2, but failed to reduce the luciferase activity of prom dmut (Figure 6G, right). Overexpression of HDAC1 reduced the expression of CSE in HUVECs, and simultaneous knockdown of ZEB2 attenuated this effect, indicating that HDAC1 represses gene expression in a ZEB2-dependent manner (Figure 6H). The chromatin immunoprecipitation assay accordingly revealed that the knockdown of ZEB2 reduced Ang II–induced binding of HDAC1 to the *CTH* promoter (Figure 6I). Coimmunoprecipitation confirmed that the knockdown of ZEB2 inhibited the formation of the HDAC1-NuRD complex (Figure 6J) and reduced the activity of the PERK signaling pathway (Figure S5H). These data collectively suggest that the ZEB2-HDAC1-NuRD complex represses CSE expression.

Reduced TRIM21-Mediated Proteasomal Degradation Results in Elevation of HDAC1

We next investigated the mechanism by which HDAC1 is upregulated in ECs in AAD. The mRNA level of HDAC1 remained unchanged in HUVECs treated with Ang II (Figure S6A). However, the protein level of HDAC1 was markedly increased by MG132 treatment, a proteasome inhibitor, rather than by an inhibitor of lysosome-dependent protein degradation (chloroquine) or autophagy-dependent protein degradation (3-MA [3-methyladenine]; Figure S6B). In addition, ubiquitination of HDAC1 was reduced by Ang II treatment, indicating a mechanism for ubiquitin-dependent degradation of HDAC1 (Figure S6C). On the basis of previous reports, 6 ubiquitin ligases that can regulate HDAC1 expression were chosen and their expression levels were determined. Both TRIM21
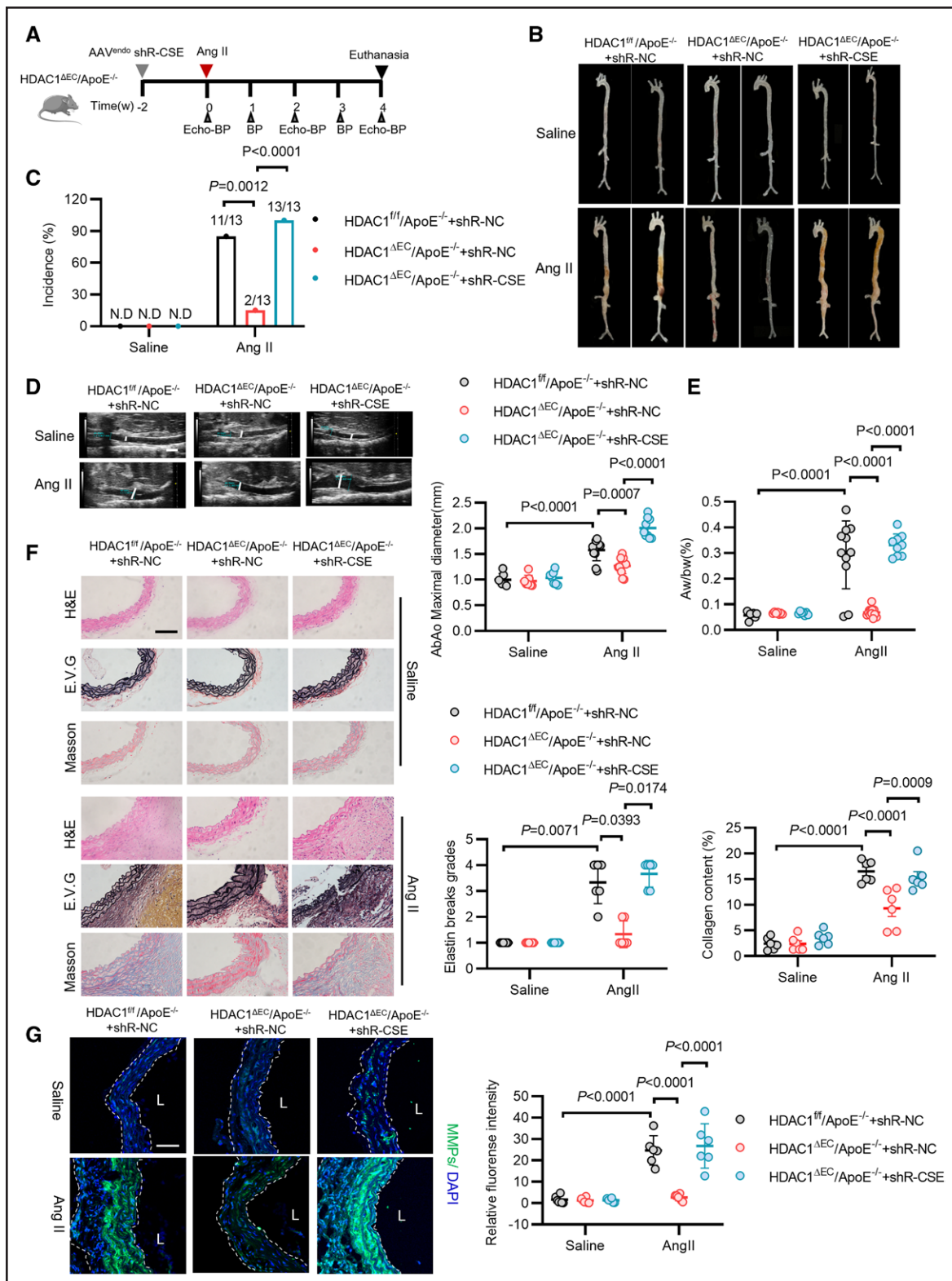
Figure 7. Deficiency of endothelial HDAC1 alleviates aortic aneurysm and dissection through regulating cystathionine γ lyase and protein disulfide isomerase S-sulfhydration.

A, Experimental design. Six-week-old HDAC1 (histone deacetylase 1)$^{flox/flox}$/ApoE$^{−/−}$ (HDAC1$^{f/f}$/ApoE$^{−/−}$) mice or endothelium-specific HDAC1 knockout ApoE$^{−/−}$ mice (HDAC1^{ΔEC}/apoE$^{−/−}$) were intravenously injected with the endothelial cell (EC)–enhanced adeno-associated virus (AAV) vector encoding negative control shRNA (shR-NC) or shRNA targeting cystathionine γ lyase (CSE; shR-CSE). After transfection for 2 weeks, mice were infused with saline or angiotensin II (Ang II; 1000 ng/kg/min) for 4 weeks, monitored for aortic dilation and blood pressure (Echo-BP), and euthanized at the indicated time point. **B**, Representative photographs (*Continued*)
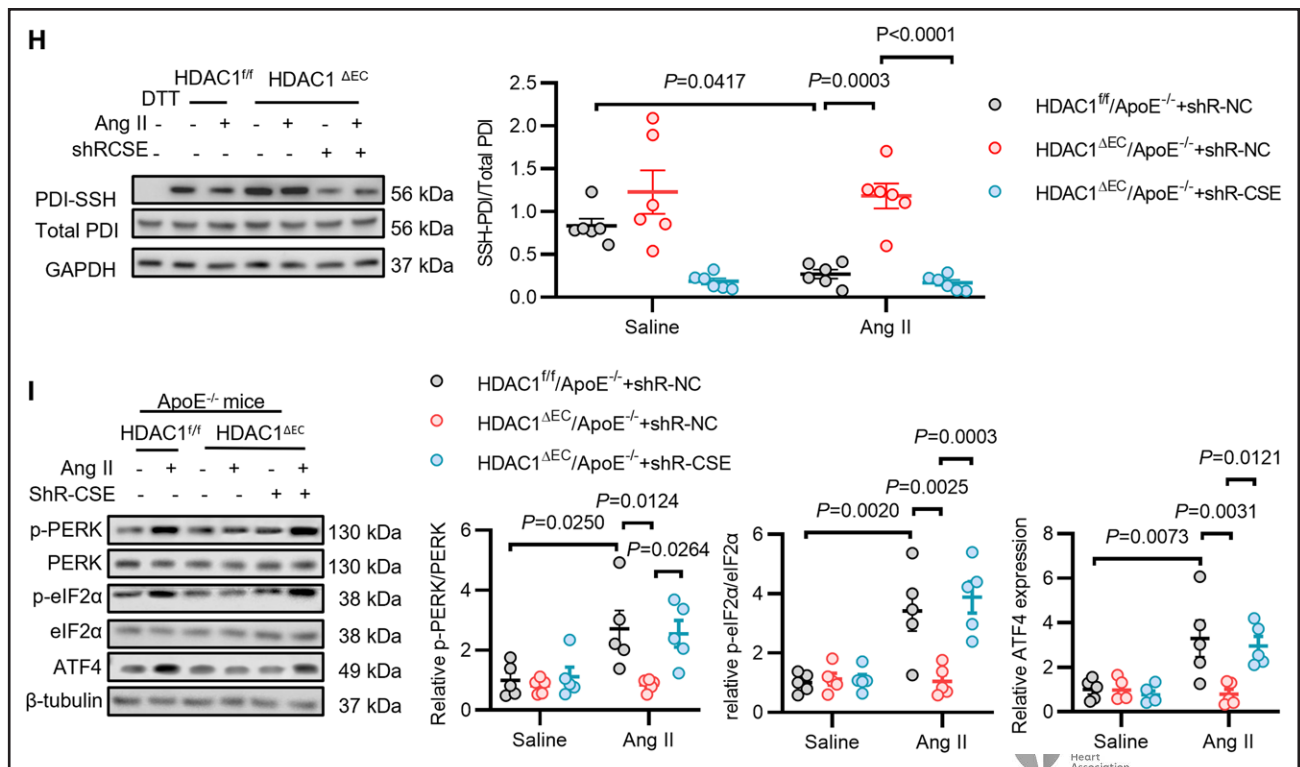
Figure 7 Continued. of aortas in each group and incidence of aortic aneurysm and dissection in each group (**C**); Fisher exact test. **D**, Representative ultrasound images (**left**), quantification of the maximal abdominal aorta (AbAo) diameters (**right**), and (**E**) statistical results of the ratio of aortic weight to body weight (Aw/bw) of HDAC1$^{f/f}$/ApoE$^{−/−}$+shR-NC+saline (n=7), HDAC1$^{f/f}$/ApoE$^{−/−}$+shR-NC+Ang II (n=11), HDAC1^{ΔEC}/ApoE$^{−/−}$+shR-NC+saline (n=7), HDAC1^{ΔEC}/ApoE$^{−/−}$+shR-NC+Ang II (n=12), HDAC1^{ΔEC}/ApoE$^{−/−}$+shR-CSE+saline (n=7), and HDAC1^{ΔEC}/ApoE$^{−/−}$+shR-CSE+Ang II (n=9) mice; 2-way ANOVA followed by Tukey multiple comparisons test. **F**, Representative hematoxylin & eosin (H&E), elastic van Gieson (EVG), and Masson trichrome staining of AbAo sections. **Right**, quantification of grade of aortic elastic fiber fragmentation and collagen content. Scale bar=100 μm; 6 in each group; Kruskal-Wallis followed by Dunn multiple comparisons test for elastic fiber fragmentation; 2-way ANOVA followed by Tukey multiple comparisons test for collagen content. **G**, Representative immunofluorescence staining for matrix metalloproteinase (MMP) activity in the abdominal aortas from differently treated mice. Scale bar=50 μm. **Right**, quantification of MMP fluorescence intensity; 6 in each group; 2-way ANOVA followed by Tukey multiple comparisons test. **H**, Representative Western blotting (**left**) and quantification of S-sulfhydration of protein disulfide isomerase (PDI-SSH; **right**) in aortas from HDAC1$^{f/f}$/ApoE$^{−/−}$+shR-NC+saline, HDAC1$^{f/f}$/ApoE$^{−/−}$+shR-NC+Ang II, HDAC1^{ΔEC}/ApoE$^{−/−}$+shR-NC+saline, HDAC1^{ΔEC}/ApoE$^{−/−}$+shR-NC+Ang II, HDAC1^{ΔEC}/ApoE$^{−/−}$+shR-CSE+saline, and HDAC1^{ΔEC}/ApoE$^{−/−}$+shR-CSE+Ang II mice; 6 distinct samples for each group 2-way ANOVA followed by Tukey multiple comparisons test. **I**, Representative Western blotting (**left**) and quantification of PERK (protein kinase RNA-like endoplasmic reticulum kinase) signaling pathway protein levels (**right**) in aortas from HDAC1$^{f/f}$/ApoE$^{−/−}$+shR-NC+saline, HDAC1$^{f/f}$/ApoE$^{−/−}$+shR-NC+Ang II, HDAC1^{ΔEC}/ApoE$^{−/−}$+shR-NC+saline, HDAC1^{ΔEC}/ApoE$^{−/−}$+shR-NC+Ang II, HDAC1^{ΔEC}/ApoE$^{−/−}$+shR-CSE+saline, and HDAC1^{ΔEC}/ApoE$^{−/−}$+shR-CSE+Ang II mice; 5 distinct samples for each group; 2-way ANOVA followed by Tukey multiple comparisons test. Data presented as mean±SD. ATF4 indicates activating transcription factor 4; eIF2α, eukaryotic translation initiation factor 2A; L, lumen; ND, not detected; p-eIF2α, phospho−eukaryotic translation initiation factor 2A; and p-PERK, phospho−protein kinase RNA-like endoplasmic reticulum kinase.

(tripartite motif containing 21) and SUMO1 (small ubiquitin-like modifier 1) were highly expressed in HUVECs (Figure S6D), and TRIM21 was also found to interact with HDAC1, according to our coimmunoprecipitation combined with mass spectrometry data. Knockdown of TRIM21 significantly increased HDAC1 levels (Figure S6E). In contrast, overexpression of TRIM21 dose-dependently reduced HDAC1 expression, and this effect was inhibited by MG132 (Figure S6F). Coimmunoprecipitation confirmed the interaction between endogenous HDAC1 and TRIM21, which was reduced by Ang II treatment (Figure S6G). These data collectively demonstrate that TRIM21-mediated ubiquitination regulates the expression of HDAC1.

EC-Specific Knockout of HDAC1 Alleviates AAD Formation by Increasing PDI-SSH

To determine whether HDAC1 reduces the expression of CSE and ultimately induces AAD in vivo, we constructed EC-specific HDAC1 knockout mice in an ApoE$^{−/−}$ background (HDAC1^{ΔEC}/ApoE$^{−/−}$) by crossing the HDAC1$^{f/f}$/ApoE$^{−/−}$ mice with the VE-Cadherin-Cre/ApoE$^{−/−}$ mice. En face staining confirmed successful knockout of HDAC1 in the endothelium and Western blotting also showed loss of HDAC1 expression in isolated mouse aortic endothelial cells of the HDAC1^{ΔEC}ApoE$^{−/−}$ mice (Figure S7A and S7B). Tail vein injections of the AAV^{endo}-shR-CSE were conducted to knockdown the
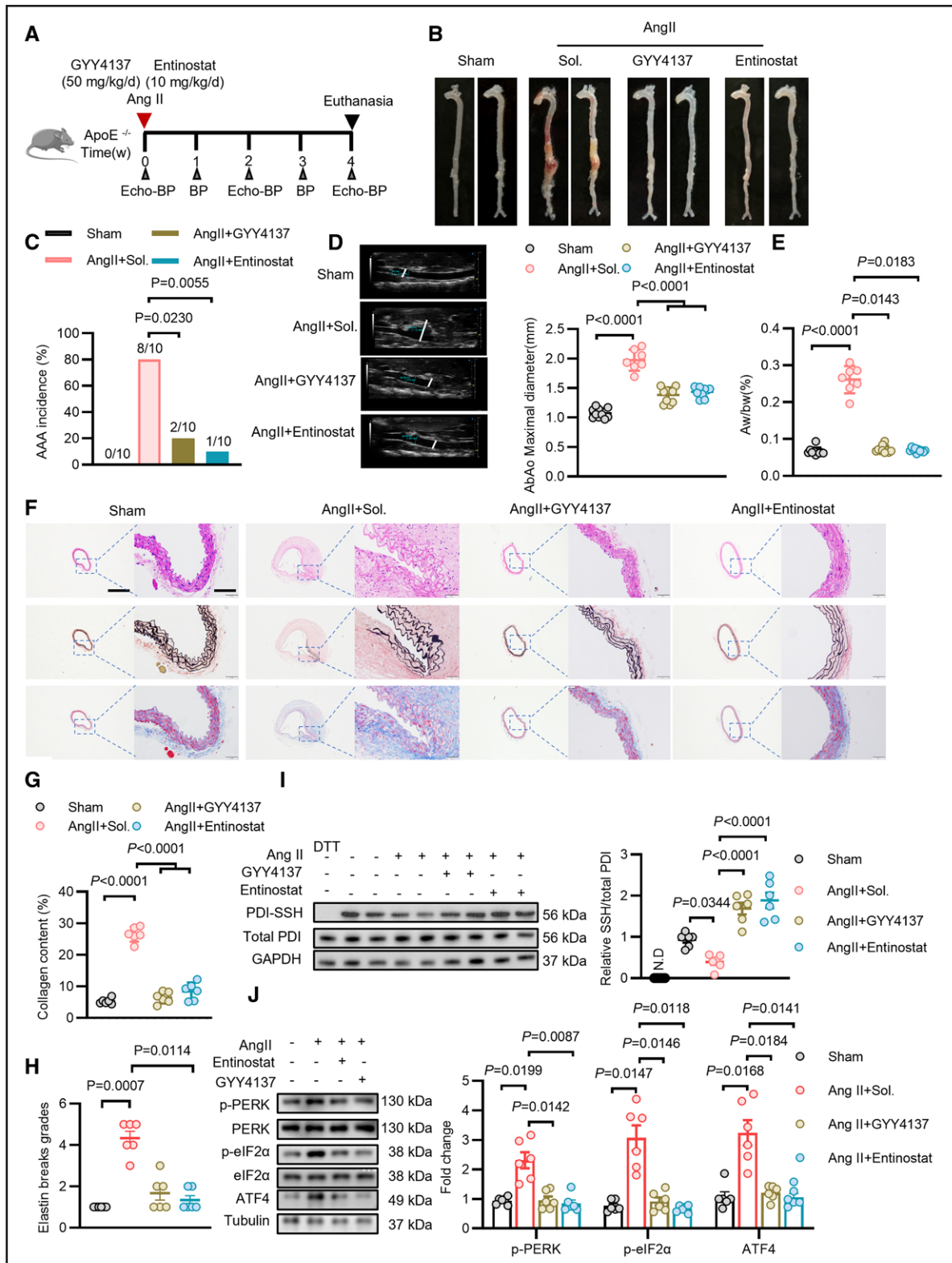
Figure 8. Both GYY4137 and entinostat alleviate aortic aneurysm and dissection.
A, Experimental design. Eight-week-old ApoE$^{-/-}$ mice were infused with saline or angiotensin II (Ang II; 1000 ng/kg/min) and intraperitoneally injected with hydrogen sulfide (H$_2$S) donor GYY4137 (50 mg/kg/day) or the HDAC1 (histone deacetylase 1) inhibitor entinostat (10 mg/kg/day) for 4 weeks. Mice were monitored for aortic dilation and blood pressure (echo-BP) and euthanized at the indicated time point. **B**, Representative photographs of aortas in each group after Ang II treatment for 28 days. **C**, Incidence of aortic aneurysm and dissection for each group; Fisher exact test. **D**, Representative ultrasound images and quantification of the maximal abdominal aorta (AbAo) diameters from sham (n=10), Ang II+solution (Sol; n=7), Ang II+ GYY4137 (n=10), and Ang II+entinostat mice (n=10). Scale bar=1 mm; ordinary 1-way (*Continued*)

Figure 8 Continued. ANOVA with Tukey multiple comparisons test. **E**, Statistical results of the ratio of aortic weight to body weight (Aw/bw) of sham (n=10), Ang II+Sol (n=7), Ang II+GYY4137 (n=10), and Ang II+entinostat mice (n=10); Kruskal-Wallis followed by Dunn multiple comparisons test. **F**, Representative hematoxylin & eosin (H&E), EVG, and Masson trichrome staining of suprarenal AoAb sections. Scale bar=1 mm (**left**) and 100 μm (**right**). **G**, The quantification of collagen content and (**H**) grade of aortic elastic fiber fragmentation; 6 in each group; for collagen content, ordinary 1-way ANOVA with Tukey multiple comparisons test was used; for elastin breaks grades, Kruskal-Wallis followed by Dunn multiple comparisons test was used. **I**, Representative Western blotting (**left**) and quantification of S-sulfhydration (SSH) of protein disulfide isomerase (PDI; **right**); 6 per group; ordinary 1-way ANOVA with Tukey multiple comparisons test. **J**, Representative Western blotting (**left**) and quantification of PERK (protein kinase RNA-like endoplasmic reticulum kinase) signaling pathway protein levels (**right**); 6 per group; data presented as mean±SD. AAA indicates abdominal aortic aneurysm; ATF4, activating transcription factor 4; DTT, dithiothreitol; eIF2α, eukaryotic translation initiation factor 2A; ND, not detected; p-eIF2α, phospho−eukaryotic translation initiation factor 2A; and p-PERK, phospho−protein kinase RNA-like endoplasmic reticulum kinase.

expression of endothelial CSE in the HDAC1$^{\Delta EC}$ApoE$^{-/-}$ mice (HDAC$^{\Delta EC}$/ApoE$^{-/-}$+shR-CSE). The AAD model was induced by subcutaneous infusion of Ang II using a minipump. The experimental procedure is shown in Figure 7A. En face staining confirmed that the EC-specific knockout of HDAC1 increased the level of CSE in the endothelium, which was reduced by transfection with AAV^{endo}-shR-CSE (Figure S7C). The level of H$_2$S in the plasma of HDAC1$^{\Delta EC}$ mice increased significantly compared with that of the HDAC1$^{f/f}$ mice and transfection of AAV^{endo}-shR-CSE reduced plasma H$_2$S levels (Figure S7D). Knockout of HDAC1 in endothelium reduced AAAs and lethal AoD and simultaneous knockdown of CSE reversed this protective effect (HDAC1$^{f/f}$/ApoE$^{-/-}$+Ang II, 11/13; HDAC1$^{\Delta EC}$/ApoE$^{-/-}$+Ang II, 2/13; HDAC1$^{\Delta EC}$/ApoE$^{-/-}$+shR-CSE+Ang II, 13/13; Figure 7B and 7C). Consistent with these findings, the maximal abdominal aortic diameter and ratio of abdominal aortic to body weight were substantially decreased in the HDAC1$^{\Delta EC}$/ApoE$^{-/-}$ mice, which was reversed with transfection of AAV^{endo}-sh-CSE (Figure 7D and 7E). The diameters of thoracic aorta, ascending aorta, and transaortic arch were increased in HDAC1$^{f/f}$/ApoE$^{-/-}$+Ang II mice and only dilation of transaortic arch was alleviated by EC-specific knockout of HDAC1. Knockdown of CSE in the endothelium, however, increased the diameters of the transaortic arch (Figure S7E through S7H). Moreover, Ang II−infused HDAC1$^{\Delta EC}$/ApoE$^{-/-}$ mice showed a reduced maximal external diameter of the suprarenal aorta than HDAC1$^{f/f}$/ApoE$^{-/-}$ mice; this protective effect was reversed by transfection of AAV^{endo}-sh-CSE (Figure S7I). Endothelium-specific knockout of HDAC1 reduced the elevation of aortic medial thickness, fragmentation of elastic fibers, deposition of collagen, and activity of matrix metalloproteinases in the suprarenal aorta; however, these beneficial effects were eliminated by EC-specific knockdown of CSE (Figure 7F and G). EC-specific knockout of HDAC1 inhibited the reduction of PDI-SSH in mice subjected to AAD, whereas knockdown of CSE in the endothelium prevented these protective effects (Figure 7H). Activation of the PERK signaling pathway was inhibited by EC-specific knockout of HDAC1 and knockdown of CSE in the endothelium prevented these protective effects (Figure 7I). These data indicate that elevation of endothelial HDAC1 aggravates AAD by reducing the expression of CSE.

Both GYY4137 and Entinostat Prevent AAD Development

We investigated the effects of GYY4137 and entinostat on the progression of AAD in mice following the protocol shown in Figure 8A. We first determined the expression of CSE in aortic tissues by en face staining and found that entinostat, rather than GYY4137, upregulated CSE expression in the endothelium (Figure S8A). GYY4137 or entinostat treatment significantly reduced AAA or lethal AoD in the ApoE$^{-/-}$ mice challenged with Ang II (Ang II+solution, 8/10; Ang II+GYY4137, 2/10; Ang II+entinostat, 1/10; Figure 8B and 8C). The maximal abdominal aortic diameter and ratio of abdominal aortic to body weight were substantially decreased with GYY4137 or entinostat treatment (Figure 8D and 8E) and no differences in the diameters of thoracic aorta, ascending aorta, descending aorta, or transaortic arch were observed in the different groups (Figure S8B through S8E). Moreover, Ang II−infused ApoE$^{-/-}$ mice showed a larger maximal external diameter of the suprarenal aorta than saline-infused mice, which was significantly reduced in mice treated with entinostat or GYY4137 (Figure S8F). Entinostat and GYY4137 treatment reduced aortic wall thickness and alleviated degradation of elastic fibers and deposition of interstitial fibrosis (Figure 8F through 8H). In situ zymography also revealed that treatment with GYY4137 and entinostat reduced matrix metalloproteinase activity (Figure S8G). The tag-switch showed that treatment with entinostat or GYY4137 effectively restored the PDI-SSH in aorta of ApoE$^{-/-}$ mice treated with Ang II (Figure 8I). Western blotting further confirmed that both entinostat and GYY4137 alleviated the activation of the PERK signaling pathway, indicating reduced ER stress (Figure 8J). Ang II−infused ApoE$^{-/-}$ mouse aorta showed reduced cGMP level and impaired ACh-induced endothelial-dependent relaxation (Figure S8H and S8I). Entinostat or GYY4137 treatment increased the cGMP concentration in mice and restored the impaired endothelial-dependent relaxation in the aortae from the Ang II−infused ApoE$^{-/-}$ mouse (Figure S8H and S8I). These data clearly indicated the protective effects of GYY4137 and entinostat against the progression of AAD.

DISCUSSION

Degeneration of endothelium drives AAD progression. However, the mechanisms underlying endothelial dysfunction during AAD remain unclear. The current study revealed the dysregulation of protein S-sulfhydration in ECs during the progression of AAD. The reduction in protein S-sulfhydration in the endothelium is induced by ZEB2-HDAC1-NuRD complex–mediated dysfunction of the CSE/H$_2$S system. Restoration of protein S-sulfhydration by increasing CSE/H$_2$S or inhibiting the ZEB2-HDAC1-NuRD complex alleviates AAD.

Endothelial cells that line the blood vessels are particularly sensitive to oxidative stress, mechanical stretching, and neurohormonal factors. The S-sulfhydration on thiols of cysteines in signaling molecules regulates endothelial function in a sophisticated fashion.[11] Protein S-sulfhydration has been found to be a key mechanism to regulate endothelial oxidative stress, inflammation, and senescence.[17,23,24] We recently found that during diabetes-accelerated atherosclerosis, high glucose level and oxidized low-density lipoprotein reduced the S-sulfhydration of KEAP1 (Kelch-like ECH-associated protein 1) and released NRF2 (nuclear factor erythroid 2–related factor 2), promoting the expression of antioxidative genes in ECs.[23] In contrast, by mapping the S-sulfhydrome of ECs exposed to shear stress, Bibli et al[15] found that the most altered family of proteins were the integrins required for EC mechanotransduction.

To determine the spectrum of persulfidated proteins in ECs during AAD, a modified biotin-switch assay was performed and the enriched proteins were identified using liquid chromatography with tandem mass spectrometry. Bioinformatics analysis identified that the most altered family of proteins in ECs during AAD was the protein process in the endoplasmic reticulum, which is largely different from what was reported previously.[15] PDI-SSH was reduced during AAD and overexpression of CSE or supplementation of an exogenous H$_2$S donor could restore its level. Point mutations showed that Cys343 and Cys400 were sites for S-sulfhydration. The reductase activity of PDI is controlled by a pair of CXXC motifs, where Cys400 resides in 1 of these motifs. On the other hand, Cys343 resides in the b′ domain of PDI, which is the substrate binding domain of PDI.[19] The dieosin-diglutathione assay, ANS binding assay, and limited proteolysis assay confirmed that both the reductase and substrate-binding activities of PDI relied on its S-sulfhydration. During the progression of AAD, PDI-SSH was significantly reduced, leading to reduced PDI activity and activation of the PERK signaling pathway.

In the cardiovascular system, CSE-derived H$_2$S is the main source of protein S-sulfhydration. CSE is mainly expressed in the ECs and is attributed to circulating H$_2$S.[25,26] A meta-analysis of existing single-cell RNA sequencing data from murine ECs confirmed the presence of CSE in the endothelium (www.ebi.ac.uk/gxa/sc/home). We found that reduced plasma H$_2$S levels were associated with AoD. In accordance, mice with endothelial CSE deficiency are vulnerable to Ang II–induced AAD, and overexpression of CSE in the endothelium retards the progression of AAD. Because there are contradictory phenotypes of blood pressure changes in CSE knockout mice,[26,27] conditional CSE knockout mice (CSE$^{\Delta EC}$), rather than systemic knockout mice, were used in our study. Long-term continuous blood pressure measurement found no alteration in SBP in the CSE$^{\Delta EC}$ mice compared with that in CSE$^{f/f}$ littermates, indicating that the effects of CSE on AAD are independent of blood pressure regulation.

Recent work using single-cell sequencing indicated the enrichment of ZEB2 in injured cardiomyocytes.[28] ZEB2 reduces the expression of target genes by recruiting corepressor complexes, such as CTBP (C-terminal binding protein).[29] It recently was reported that ZEB2 represses Notch signaling during peripheral nerve development.[30] Through the combined use of coimmunoprecipitation and liquid chromatography with tandem mass spectrometry, we found that ZEB2 recruited HDAC1 and the NuRD corepressor complex under the condition of AAD. Knockdown of ZEB2 impedes the formation of the HDAC1-NuRD complex and leads to increased expression of CSE. Mutations in the predicted ZEB2 binding motifs in the *CTH* promoter relieved the inhibitory effects. To our knowledge, this is the first study showing that ZEB2 transcriptionally represses CSE and regulates protein S-sulfhydration. Although a similar study showed that the expression of HDAC1 is higher in the aortic wall of patients with AAD,[31] we found that the increased level of HDAC1 in the ECs, rather than in the smooth muscle cells, induces the progression of AAD through a distinct mechanism that has not been discovered before.

This study has some limitations. Recent evidence suggests that GYY4137 and entinostat may prevent the occurrence and progression of AAD, and whether they can slow down the progression of AAD in mice with aneurysms remains to be investigated. Further investigations to confirm the treatment values are essential for bringing these interventions to the clinic.

The current study investigated endothelial S-sulfhydration during AAD and highlights the role of endothelial PDI-SSH in protecting against the progression of AAD. The study also found that the ZEB2-HDAC1-NuRD complex represses PDI-SSH through transcriptional inhibition of the CSE/H$_2$S system. This study identified that reduced plasma H$_2$S levels are associated with AoD and provides evidence for the effectiveness of managing the ZEB2-HDAC1-NuRD complex and CSE/H$_2$S axis in AAD prevention and treatment.

ARTICLE INFORMATION

Affiliations

Key Laboratory of Cardiovascular and Cerebrovascular Medicine, Key Laboratory of Targeted Intervention of Cardiovascular Disease, Collaborative Innovation Center for Cardiovascular Disease Translational Medicine, the Affiliated Suzhou Hospital of Nanjing Medical University, Suzhou Municipal Hospital, Gusu School (S.L., C.K., S.Z., Xin Tang, Y.W., X.Z., R.L., X.L., S.S., A.G., L.X., Y.J.), and Department of Forensic Medicine (F.C.), Nanjing Medical University, China. Department of Thoracic and Cardiovascular Surgery, the Affiliated Drum Tower Hospital of Nanjing University Medical School, Nanjing Drum Tower Hospital Clinical College of Nanjing Medical University, Institute of Cardiothoracic Vascular Disease, Nanjing University, China (Xinlong Tang, W.X., D.W.). Department of Pharmacology (State-Province Key Laboratories of Biomedicine-Pharmaceutics of China), College of Pharmacy, Key Laboratory of Cardiovascular Medicine Research and Key Laboratory of Myocardial Ischemia, Chinese Ministry of Education, Harbin Medical University, Heilongjiang, China (Z.-R.Z., Y.J.). NHC Key Laboratory of Cell Transplantation, the Central Laboratory of the First Affiliated Hospital, Harbin Medical University, Heilongjiang, China (Z.-R.Z., Y.J.). CAS Key Laboratory of Tissue Microenvironment and Tumor, Shanghai Institute of Nutrition and Health, Chinese Academy of Sciences, China (Q.J.). Center for Metabolic Disease Research, Department of Microbiology and Immunology, Temple University Lewis Katz School of Medicine, Philadelphia, PA (H.W.). Department of Geriatrics, First Affiliated Hospital of Nanjing Medical University, China (Y.H.).

Supplemental Material

Expanded Methods
Tables S1–S3
Figures S1–S8
References 32–40

REFERENCES

1. Pi X, Xie L, Patterson C. Emerging roles of vascular endothelium in metabolic homeostasis. *Circ Res.* 2018;123:477–494. doi: 10.1161/CIRCRESAHA.118.313237
2. Shen YH, LeMaire SA, Webb NR, Cassis LA, Daugherty A, Lu HS. Aortic aneurysms and dissections series. *Arterioscler Thromb Vasc Biol.* 2020;40:e37–e46. doi: 10.1161/ATVBAHA.120.313991
3. Famularo M, Meyermann K, Lombardi JV. Aneurysmal degeneration of type B aortic dissections after thoracic endovascular aortic repair: a systematic review. *J Vasc Surg.* 2017;66:924–930. doi: 10.1016/j.jvs.2017.06.067
4. Koo HK, Lawrence KA, Musini VM. Beta-blockers for preventing aortic dissection in Marfan syndrome. *Cochrane Database Syst Rev.* 2017;11:CD011103. doi: 10.1002/14651858.CD011103.pub2
5. Siordia JA. Beta-blockers and abdominal aortic aneurysm growth: a systematic review and meta-analysis. *Curr Cardiol Rev.* 2021;17:e230421187502. doi: 10.2174/1573403X16999201102213619
6. Pitcher A, Spata E, Emberson J, Davies K, Halls H, Holland L, Wilson K, Reith C, Child AH, Clayton T, et al; Marfan Treatment Trialists' Collaboration. Angiotensin receptor blockers and beta blockers in Marfan syndrome: an individual patient data meta-analysis of randomised trials. *Lancet.* 2022;400:822–831. doi: 10.1016/S0140-6736(22)01534-3
7. van Andel MM, Indrakusuma R, Jalalzadeh H, Balm R, Timmermans J, Scholte AJ, van den Berg MP, Zwinderman AH, Mulder BJM, de Waard V, et al. Long-term clinical outcomes of losartan in patients with Marfan syndrome: follow-up of the multicentre randomized controlled COMPARE trial. *Eur Heart J.* 2020;41:4181–4187. doi: 10.1093/eurheartj/ehaa377
8. Rateri DL, Moorleghen JJ, Balakrishnan A, Owens AP 3rd, Howatt DA, Subramanian V, Poduri A, Charnigo R, Cassis LA, Daugherty A. Endothelial cell-specific deficiency of Ang II type 1a receptors attenuates Ang II-induced ascending aortic aneurysms in LDL receptor−/− mice. *Circ Res.* 2011;108:574–581. doi: 10.1161/CIRCRESAHA.110.222844
9. Fan LM, Douglas G, Bendall JK, McNeill E, Crabtree MJ, Hale AB, Mai A, Li JM, McAteer MA, Schneider JE, et al. Endothelial cell-specific reactive oxygen species production increases susceptibility to aortic dissection. *Circulation.* 2014;129:2661–2672. doi: 10.1161/CIRCULATIONAHA.113.005062
10. Franck G, Dai J, Fifre A, Ngo S, Justine C, Michineau S, Allaire E, Gervais M. Reestablishment of the endothelial lining by endothelial cell therapy stabilizes experimental abdominal aortic aneurysms. *Circulation.* 2013;127:1877–1887. doi: 10.1161/CIRCULATIONAHA.113.001677
11. Bibli SI, Fleming I. Oxidative post-translational modifications: a focus on cysteine S-sulfhydration and the regulation of endothelial fitness. *Antioxid Redox Signal.* 2021;35:1494–1514. doi: 10.1089/ars.2021.0162
12. Weerapana E, Wang C, Simon GM, Richter F, Khare S, Dillon MB, Bachovchin DA, Mowen K, Baker D, Cravatt BF. Quantitative reactivity profiling predicts functional cysteines in proteomes. *Nature.* 2010;468:790–795. doi: 10.1038/nature09472
13. Jiang S, Xu W, Chen Z, Cui C, Fan X, Cai J, Gong Y, Geng B. Hydrogen sulfide reduces hyperhomocysteinaemia-induced endothelial ER stress by sulfhydrating protein disulphide isomerase to attenuate atherosclerosis. *J Cell Mol Med.* 2021;25:3437–3448. doi: 10.1111/jcmm.16423
14. Kimura H. Physiological roles of hydrogen sulfide and polysulfides. *Handb Exp Pharmacol.* 2015;230:61–81. doi: 10.1007/978-3-319-18144-8_3
15. Bibli SI, Hu J, Looso M, Weigert A, Ratiu C, Wittig J, Drekolia MK, Tombor L, Randriamboavonjy V, Leisegang MS, et al. Mapping the endothelial cell S-sulfhydrome highlights the crucial role of integrin sulfhydration in vascular function. *Circulation.* 2021;143:935–948. doi: 10.1161/CIRCULATIONAHA.120.051917
16. Lu H, Howatt DA, Balakrishnan A, Graham MJ, Mullick AE, Daugherty A. Hypercholesterolemia Induced by a PCSK9 gain-of-function mutation augments angiotensin II-induced abdominal aortic aneurysms in C57BL/6 mice: brief report. *Arterioscler Thromb Vasc Biol.* 2016;36:1753–1757. doi: 10.1161/ATVBAHA.116.307613
17. Bibli SI, Hu J, Sigala F, Wittig I, Heidler J, Zukunft S, Tsilimigras DI, Randriamboavonjy V, Wittig J, Kojonazarov B, et al. Cystathionine gamma lyase sulfhydrates the RNA binding protein human antigen R to preserve endothelial cell function and delay atherogenesis. *Circulation.* 2019;139:101–114. doi: 10.1161/CIRCULATIONAHA.118.034757
18. Shergalis AG, Hu S, Bankhead A 3rd, Neamati N. Role of the ERO1-PDI interaction in oxidative protein folding and disease. *Pharmacol Ther.* 2020;210:107525. doi: 10.1016/j.pharmthera.2020.107525
19. Bekendam RH, Bendapudi PK, Lin L, Nag PP, Pu J, Kennedy DR, Feldenzer A, Chiu J, Cook KM, Furie B, et al. A substrate-driven allosteric switch that enhances PDI catalytic activity. *Nat Commun.* 2016;7:12579. doi: 10.1038/ncomms12579
20. Raturi A, Mutus B. Characterization of redox state and reductase activity of protein disulfide isomerase under different redox environments using a sensitive fluorescent assay. *Free Radic Biol Med.* 2007;43:62–70. doi: 10.1016/j.freeradbiomed.2007.03.025
21. Yu J, Li T, Liu Y, Wang X, Zhang J, Wang X, Shi G, Lou J, Wang L, Wang CC, et al. Phosphorylation switches protein disulfide isomerase activity to maintain proteostasis and attenuate ER stress. *EMBO J.* 2020;39:e103841. doi: 10.15252/embj.2019103841
22. Chao ML, Luo S, Zhang C, Zhou X, Zhou M, Wang J, Kong C, Chen J, Lin Z, Tang X, et al. S-nitrosylation-mediated coupling of G-protein alpha-2 with CXCR5 induces Hippo/YAP-dependent diabetes-accelerated atherosclerosis. *Nat Commun.* 2021;12:4452. doi: 10.1038/s41467-021-24736-y
23. Xie L, Gu Y, Wen M, Zhao S, Wang W, Ma Y, Meng G, Han Y, Wang Y, Liu G, et al. Hydrogen sulfide induces Keap1 S-sulfhydration and suppresses diabetes-accelerated atherosclerosis via Nrf2 activation. *Diabetes.* 2016;65:3171–3184. doi: 10.2337/db16-0020
24. Das A, Huang GX, Bonkowski MS, Longchamp A, Li C, Schultz MB, Kim LJ, Osborne B, Joshi S, Lu Y, et al. Impairment of an endothelial NAD(+)-H2S signaling network is a reversible cause of vascular aging. *Cell.* 2018;173:74–89.e20. doi: 10.1016/j.cell.2018.02.008
25. Polhemus DJ, Lefer DJ. Emergence of hydrogen sulfide as an endogenous gaseous signaling molecule in cardiovascular disease. *Circ Res.* 2014;114:730–737. doi: 10.1161/CIRCRESAHA.114.300505

26. Yang G, Wu L, Jiang B, Yang W, Qi J, Cao K, Meng Q, Mustafa AK, Mu W, Zhang S, et al. H2S as a physiologic vasorelaxant: hypertension in mice with deletion of cystathionine gamma-lyase. *Science*. 2008;322:587–590. doi: 10.1126/science.1162667

27. Szijarto IA, Marko L, Filipovic MR, Miljkovic JL, Tabeling C, Tsvetkov D, Wang N, Rabelo LA, Witzenrath M, Diedrich A, et al. Cystathionine gamma-lyase-produced hydrogen sulfide controls endothelial NO bioavailability and blood pressure. *Hypertension*. 2018;71:1210–1217. doi: 10.1161/HYPERTENSIONAHA.117.10562

28. Gladka MM, Kohela A, Molenaar B, Versteeg D, Kooijman L, Monshouwer-Kloots J, Kremer V, Vos HR, Huibers MMH, Haigh JJ, et al. Cardiomyocytes stimulate angiogenesis after ischemic injury in a ZEB2-dependent manner. *Nat Commun*. 2021;12:84. doi: 10.1038/s41467-020-20361-3

29. Postigo AA, Depp JL, Taylor JJ, Kroll KL. Regulation of Smad signaling through a differential recruitment of coactivators and corepressors by ZEB proteins. *EMBO J*. 2003;22:2453–2462. doi: 10.1093/emboj/cdg226

30. Wu LM, Wang J, Conidi A, Zhao C, Wang H, Ford Z, Zhang L, Zweier C, Ayee BG, Maurel P, et al. Zeb2 recruits HDAC-NuRD to inhibit Notch and controls Schwann cell differentiation and remyelination. *Nat Neurosci*. 2016;19:1060–1072. doi: 10.1038/nn.4322

31. Sun L, Wang C, Yuan Y, Guo Z, He Y, Ma W, Zhang J. Downregulation of HDAC1 suppresses media degeneration by inhibiting the migration and phenotypic switch of aortic vascular smooth muscle cells in aortic dissection. *J Cell Physiol*. 2020;235:8747–8756. doi: 10.1002/jcp.29718

32. Wang L, Luo JY, Li B, Tian XY, Chen LJ, Huang Y, Liu J, Deng D, Lau CW, Wan S, et al. Integrin-YAP/TAZ-JNK cascade mediates atheroprotective effect of unidirectional shear flow. *Nature*. 2016;540:579–582. doi: 10.1038/nature20602

33. Varadi K, Michelfelder S, Korff T, Hecker M, Trepel M, Katus HA, Kleinschmidt JA, Muller OJ. Novel random peptide libraries displayed on AAV serotype 9 for selection of endothelial cell-directed gene transfer vectors. *Gene Ther*. 2012;19:800–809. doi: 10.1038/gt.2011.143

34. Wang JM, Chen AF, Zhang K. Isolation and primary culture of mouse aortic endothelial cells. *J Vis Exp*. 2016;118:52965. doi: 10.3791/52965

35. Luo W, Wang Y, Zhang L, Ren P, Zhang C, Li Y, Azares AR, Zhang M, Guo J, Ghaghada KB, et al. Critical role of cytosolic DNA and its sensing adaptor STING in aortic degeneration, dissection, and rupture. *Circulation*. 2020;141:42–66. doi: 10.1161/CIRCULATIONAHA.119.041460

36. Cai D, Sun C, Zhang G, Que X, Fujise K, Weintraub NL, Chen SY. A novel mechanism underlying inflammatory smooth muscle phenotype in abdominal aortic aneurysm. *Circ Res*. 2021;129:e202–e214. doi: 10.1161/CIRCRESAHA.121.319374

37. Lee LY, Oldham WM, He H, Wang R, Mulhern R, Handy DE, Loscalzo J. Interferon-gamma impairs human coronary artery endothelial glucose metabolism by tryptophan catabolism and activates fatty acid oxidation. *Circulation*. 2021;144:1612–1628. doi: 10.1161/CIRCULATIONAHA.121.053960

38. Li C, Liu ZH, Chen JW, Shu XY, Shen Y, Ding FH, Zhang RY, Shen WF, Lu L, Wang XQ. Using en face immunofluorescence staining to observe vascular endothelial cells directly. *J Vis Exp*. 2019;150:59325. doi: 10.3791/59325

39. Ditroi T, Nagy A, Martinelli D, Rosta A, Kozich V, Nagy P. Comprehensive analysis of how experimental parameters affect H2S measurements by the monobromobimane method. *Free Radic Biol Med*. 2019;136:146–158. doi: 10.1016/j.freeradbiomed.2019.04.006

40. Zhao S, Song T, Gu Y, Zhang Y, Cao S, Miao Q, Zhang X, Chen H, Gao Y, Zhang L, et al. Hydrogen sulfide alleviates liver injury through the S-sulfhydrated-Kelch-like ECH-associated protein 1/nuclear erythroid 2-related factor 2/low-density lipoprotein receptor-related protein 1 pathway. *Hepatology*. 2021;73:282–302. doi: 10.1002/hep.31247